Chapter 20
Applications of Magnetic Nanoparticles in Biomedicine

Carlos Bárcena, Amandeep K. Sra, and Jinming Gao

Abstract In recent years, magnetic nanoparticles have played an increasing role in biomedical applications and have been the subject of extensive research investigations. Physical properties, including nanoparticle size, composition, and surface chemistry, vary widely and influence their biological and pharmacological properties and, ultimately, their clinical applications. Among different magnetic nanoparticles, superparamagnetic iron oxide nanoparticles (SPIOs) were found nontoxic and used as magnetic resonance imaging (MRI) contrast agents, in molecular and cellular imaging applications. SPIOs are used in detection of liver metastases, metastatic lymph nodes, and inflammatory and/or neural degenerative diseases. In addition, drug delivery via magnetic targeting, hyperthermia, and labeling/ tracking of stem cells have also been explored as potential therapeutic options.

20.1 Introduction

The use of magnetic particles in medicine has long been recorded since ancient times [69]. Often regarded as the first philosopher in the Greek tradition, Thales of Miletus (ca. 624–547 BC) believed man and magnet were somehow connected and each possessed a soul. Hippocrates of Kos (ca. 460–370 BC), father of medicine, made medical references to magnetism. He used the styptic iron oxides magnetite and hematite to stop bleeding and control hemorrhage. In the first century, Roman scholar Pliny the Elder (23–79 AD) described the treatment of burns with pulverized magnets.

In more modern times, medical uses for magnets and magnetic particles have spread to numerous fields including dentistry, cardiology, neurology, oncology, and

J. Gao (✉)
Harold C. Simmons Comprehensive Cancer Center, University of Texas Southwestern Medical Center at Dallas, Dallas TX 75390; Department of Chemistry, University of Texas at Dallas, Richardson, TX 75080, USA
e-mail: jinming.gao@utsouthwestern.edu

J.P. Liu et al. (eds.), *Nanoscale Magnetic Materials and Applications*,
DOI 10.1007/978-0-387-85600-1_20,

radiology. In dentistry, magnets are commonly applied to aid in the retention of oral prostheses [50]. Magnetic intrauterine devices for use in contraception have recently been developed [121]. Purification of healthy bone marrow cells from tumor cell with magnetic microspheres was established ex vivo [184, 185]. Moving from the macroscale to the nanoscale, magnetic nanoparticles have found increasing use in biomedical applications. Working in unison, strong local magnets can be used to target specific organs where magnetic nanoparticles can accumulate in targeted sites for imaging and/or therapy. In magnetic resonance imaging (MRI), superparamagnetic iron oxide (SPIO) nanoparticles are used as negative contrast agents to enhance imaging contrast. Furthermore, these SPIO nanoparticles have been used as imaging probes for cell labeling and tracking throughout the human body.

Unlike bulk ferromagnetic materials, SPIO nanoparticles have no net magnetic moment until they are placed in an external magnetic field [30]. Quantum size effects and the large surface area of magnetic nanoparticles dramatically affect their magnetic properties such as exhibition of superparamagnetic phenomena and quantum tunneling effect of magnetization [61]. Therefore, based on their unique physical, chemical, thermal, and mechanical properties, SPIOs demonstrate great potential for various biomedical applications.

20.2 Nanoparticle Classification

Magnetic nanoparticles can be classified in a variety of categories based on composition and physical or biological properties. Typically, most magnetic nanoparticles for biomedical applications are comprised of iron oxide-based nano-crystalline structures of magnetite (Fe_3O_4) and/or maghemite (γ-Fe_2O_3) encased or coated with polysaccharide, organic or polymeric stabilizers, or inorganic coatings. Recently, however, novel nanoparticles with advanced magnetic properties are being actively pursued for potential biomedical applications. One such class of materials is transition metal ferrites (MFe_2O_4) nanoparticles, where M is a divalent metal ion, while others are metal alloys such as iron cobalt (FeCo) [164] or iron platinum (FePt) [42] nanoparticles.

In addition to composition, size also plays a critical role in determining the magnetic and biological properties of these nanoparticles. Focusing on clinically relevant nanoparticles, SPIO hydrodynamic diameters can vary widely depending on the type of surface modification, but the nanoparticles themselves can range from 3 to 1,000 nm in diameter. In general, SPIOs are categorized based on their overall diameter (iron oxide core and hydrated coating) including [179, 195] “large” oral SPIO agents (300 nm–3.5 μm), standard SPIO (SSPIO, 60–150 nm), ultra-small SPIO (USPIO, 10–40 nm) [198], a subset of USPIO named monocrystalline iron oxide nanoparticles (MION, 10–30 nm) to emphasize the single crystal nature of the core [165], and very small SPIO (VSOP, 7 nm) [178]. Other acronyms include cross-linked iron oxide (CLIO) [207], monodisperse iron oxide nanoparticle (variation of MION), and magnetism-engineered iron oxide (MEIO) [114]; all fall in the initial categories above.

20.3 Syntheses of SPIO Nanoparticles

Several methods are generally used to produce iron oxide nanoparticles. Historically, physical grinding of bulk magnetite with a stabilizing surfactant produced the first documented ferrofluids [136]. However, for biomedical applications, several chemical methods were established to synthesize SPIOs. Some of the more commonly used methods are co-precipitation, microemulsion, and thermal decomposition, although numerous other methods exist. The main challenge is to produce and reproduce monodisperse SPIO without any complex purification steps. Ideally, the synthetic scheme should also yield highly crystalline nanoparticles with a high saturation magnetization (M_s).

20.3.1 Co-precipitation

The most common method for producing SPIO nanoparticles is a one-step co-precipitation reaction of Fe^{2+} and Fe^{3+} salts in an alkaline solution [22, 26, 40, 63, 67, 78, 97, 101, 115, 132, 177, 205]. The precipitate is recovered through magnetic isolation or centrifugation. The overall reaction may be written as shown in Eq. (20.1) [67, 101].

$$Fe^{2+} + 2Fe^{3+} + 8OH^- \rightarrow Fe_3O_4 + 4H_2O \tag{20.1}$$

According to the thermodynamics for this reaction, a complete precipitation of Fe_3O_4 should be expected between pH 7.5 and 14, while maintaining a molar ratio of Fe^{2+}:Fe^{3+} at 1:2 under a nonoxidizing, oxygen-free environment. Otherwise, Fe_3O_4 may also be oxidized to $Fe(OH)_3$ (Eq. 20.2).

$$4Fe_3O_4 + O_2 + 18H_2O \rightarrow 12Fe(OH)_3 \tag{20.2}$$

This dramatically affects the physical and chemical properties of the nanoparticles. In order to prevent possible oxidation and aggregation, Fe_3O_4 nanoparticles are usually coated with organic or inorganic molecules during the precipitation process. The resulting precipitate is reddish brown (maghemite) to brownish black (magnetite) in color, depending on the oxidation state of iron. Maghemite is the ferrimagnetic cubic form of Fe(III) oxide and differs from the inverse spinel structure of magnetite through vacancies on the cation sublattice. However, both possess very similar lattice parameters at 8.346 and 8.396 Å for maghemite and magnetite [27, 179], respectively, making chemical identification very difficult with techniques such as x-ray diffraction. To prevent possible oxidation, the synthesis is carried out in an inert environment by bubbling inert gas through the reaction solution.

Although co-precipitation methods are widely used due to its simplicity and ability to be scaled up for large reaction, the nanoparticles produced are fairly polydisperse. Another disadvantage of these bulk solution syntheses is that the pH value of the reaction mixture needs to be adjusted during both the synthesis and the

purification steps. Advancement in the use of magnetic particles for biomedical applications depends on new synthetic methods with better control over size distribution, magnetic properties, and particle surface characteristics. As a result, other methods have been developed to synthesize nanoparticles with more uniform dimensions.

20.3.2 Microemulsion

A microemulsion is a thermodynamically stable isotropic mixture of two immiscible liquids and surfactant [141]. Microemulsions may be classified as water-in-oil (w/o) or oil-in-water (o/w) emulsion, depending on the dispersed and continuous phases. In both cases, the dispersed phase consists of monodispersed droplets ranging from 10 to 100 nm in diameter. The main advantage is that microemulsions provide compartmentalized liquid structures with high surface area. These structures then serve as versatile media for chemical reactions, where the resulting nanoparticles of desired size reflect the shape and the environment of the aqueous/organic droplets [141]. For biomedical applications, the water-in-oil approach is a more common technique for preparing highly monodisperse iron oxide nanoparticles.

The general strategy involves enclosing "nanodroplets" of aqueous metal salts in a surfactant coat that separates them from the surrounding organic solution to form reverse micelles [49, 83, 116, 117, 120, 141, 162, 193]. An alkaline solution precipitates and oxidizes the SPIO within the micelle. For example, ferric and ferrous salts are mixed with dioctyl sulfosuccinate sodium salt (AOT) and lecithin (phosphatidylcholine) in an organic hydrocarbon phase. After centrifugation to remove impurities, ammonium hydroxide/AOT solution is added to the metal/AOT mixture with stirring. The metal hydroxides are precipitated and are oxidized to ferrite within the nanosized micelle. After stirring to achieve complete conversion, the solvent is removed and the nanoparticles are re-dispersed in water (Fig. 20.1). The size of the synthesized nanoparticles is relatively uniform and can be varied from 3 to 20 nm by varying the iron salt or the surfactant concentrations.

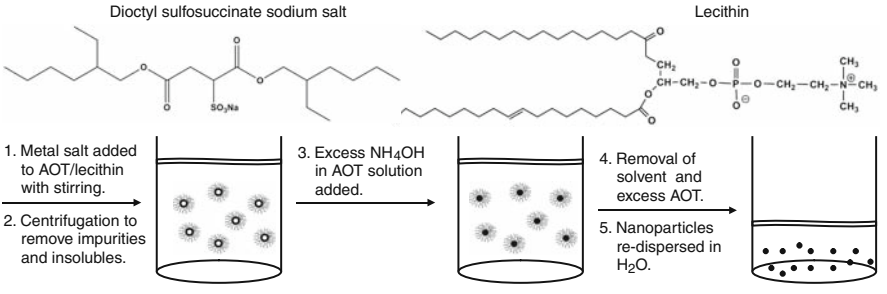

Fig. 20.1 Scheme for preparing monodisperse SPIO inside w/o microemulsion droplets

20.3.3 Thermal Decomposition

More recently, organic solution-phase decomposition of iron precursors at high temperature has been used in iron oxide nanoparticle synthesis. Advances in the synthesis process has demonstrated that direct decomposition of iron cupferron complex ($FeCup_3$, Cup: *N*-nitrosophenylhydroxylamine) [154] or decomposition of iron pentacarbonyl ($Fe(CO)_5$) [80, 139] followed by oxidation can lead to high-quality monodisperse γ-Fe_2O_3 nanoparticles. The preparation of metal cupferron complexes is based on the precipitation of a metal salt from aqueous solution at a specific pH with cupferron. The synthesis of highly crystalline and monodisperse γ-Fe_2O_3 nanoparticles also result from high temperature aging of the iron–oleic acid metal complex. This complex was prepared by thermal decomposition of $Fe(CO)_5$ in the presence of oleic acid. The resulting iron nanoparticles were transformed into monodisperse γ-Fe_2O_3 by controlled mild oxidation using trimethylamine oxide. By controlling experimental parameters, the particle size can be varied from 4 to 16 nm. However, these synthetic procedures only form γ-Fe_2O_3, not the more desired Fe_3O_4.

Sun et al. [172, 173] for the first time demonstrated that high-temperature solution phase reaction of iron(III) acetylacetonate, $Fe(acac)_3$, with 1,2-hexadecanediol in the presence of oleic acid and oleylamine can be used to make monodisperse magnetite (Fe_3O_4) nanoparticles under 20 nm. This procedure creates highly crystalline nanoparticles with high M_s (16 nm particles, ~83 emu/g) approaching 84.5 emu/g for commercial magnetite fine powder. In addition, this process can be readily extended to the synthesis of other types of ferrite (MFe_2O_4) nanoparticles, where M is a divalent metal ion (e.g., Mn^{2+}, Fe^{2+}, Co^{2+}, Ni^{2+}, Cu^{2+}, Mg^{2+}, Zn^{2+}, Cd^{2+}) [81, 95, 114, 173, 210]. The benefit of these mixed ferrite structures would be an increase in M_s due to the increased moment of the M^{2+} ion. These results were shown by Cheon et al. [114] who synthesized $NiFe_2O_4$, $CoFe_2O_4$, $FeFe_2O_4$, and $MnFe_2O_4$ and observed an increase in the transverse relaxivity coefficient, a measure of MR contrast effect, due to the increase in M_s. However, one of the major challenges for the Sun method is that the resulting nanoparticles from the initial reaction are subsequently used as seed crystals to grow larger magnetite nanoparticles, which makes scale-up for mass production tedious and possibly problematic. In addition, the cost of the starting materials for this reaction is relatively high at today's prices.

To address this issue, Hyeon et al. [138] developed an economical mass-production method to produce magnetic nanoparticles using inexpensive and nontoxic metal salts as reactants. This relatively simple procedure is shown in Fig. 20.2 (sodium-oleate = $CH_3(CH_2)_7CH{=}{=}CH(CH_2)_7COONa$).

In this reaction, an iron–oleate complex is first made by reacting iron chloride and sodium oleate. The iron–oleate complex along with oleic acid in a high boiling point solvent is then heated to 320°C. The nanoparticles are then washed and separated by centrifugation to provide monodispersed SPIO nanoparticles.

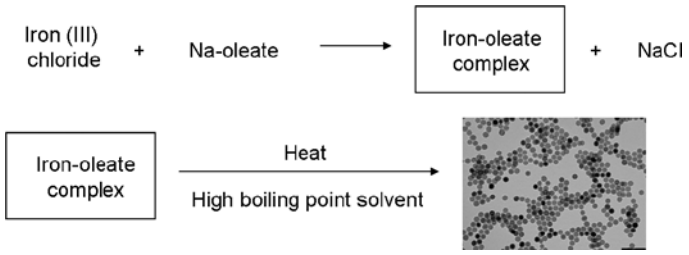

Fig. 20.2 Scheme for the mass production of SPIO (scale bar = 100 nm)

20.3.4 Alternative Methods

Other methods that exist for the controlled syntheses of SPIO particles include ultrasound sonication and spray and laser pyrolysis. During ultrasound sonication, stable ferromagnetic colloids of iron are formed using high-intensity ultrasound to sonochemically decompose volatile organometallic compounds. Volatile organometallic precursors, such as $Fe(CO)_5$, inside the cavitating bubble are decomposed in the presence of a stabilizer to create a nanosized iron colloid. The collapse of bubbles generates localized hot spots with transient temperatures of approximately 5000 K which induce particle formation [174]. In spray pyrolysis, a solution is sprayed into a series of reactors where the solute condenses as the solvent evaporates. Here in an organic compound, the Fe ions are reduced to a mixture of Fe^{2+} and Fe^{3+} ions, leading to SPIO formation [38, 122]. Pure γ-Fe_2O_3 particles are prepared by a continuous wave CO_2 laser-induced pyrolysis of $Fe(CO)_5$ vapor in an oxidizing atmosphere [188]. This synthesis method initiates and sustains a chemical reaction. Above a certain pressure and laser power, a critical concentration of product nuclei is formed in the reaction zone. Finally, another synthetic route is a layer-by-layer deposition method [48]. Chemisorption of ions allows shells or nanoparticle cores around existing particles to form by repeated submersion of a substrate or colloidal template in solution of oppositely charged polyelectrolytes.

20.4 Surface Modifications of Magnetic Nanoparticles

Pristine magnetic SPIOs are not very useful in practical applications due to their tendency to form aggregates. Also, aggregation may result in alteration of magnetic properties. Therefore, a suitable stabilizer coating is required to overcome this limitation. Stabilizers such as organic molecules, surfactants, or polymers are often added during or after synthesis to prevent aggregation of the SPIOs. However, one of the major issues that need to be addressed is the stability of these nanoparticles in a physiological aqueous environment, and the surface kinetics play a major role in this respect.

Typically, SPIOs are synthesized by two basic methodologies. In the first method, bare SPIOs are synthesized by addition of concentrated base to di- and trivalent

Fe salt solution. These bare SPIOs can then be coated in monomer and polymers through nonspecific adsorption following their purification to make them more biocompatible. Alternatively, the stabilizers can be introduced during the co-precipitation steps to prevent aggregation of the nanoscale particulate. High-temperature decomposition polyol synthesis of SPIO in the presence of fatty acids as the stabilizers yields highly crystalline and monodispersed nanoparticles. However, these as-synthesized nanoparticles are water insoluble due to the hydrophobic ligands. For biomedical applications, it is necessary to render these nanoparticles hydrophilic as the body recognizes hydrophobic particles as foreign and are rapidly taken up by the mononuclear phagocytic system (MPS) [35, 111]. Thus the goal of surface modification is to make the nanoparticles unrecognizable by the MPS and to guide them to the desired site.

20.4.1 Organic and Polymeric Stabilizers

20.4.1.1 Organic Stabilizers

Several studies have dealt with a variety of methodologies including ligand exchange, phosphine oxide polymers, and dendrons to improve the stability of SPIOs in aqueous solutions. The ligand exchange method involves adding an excess of ligand to the nanoparticle solution to displace the original ligand on the nanoparticles surface. Cheon et al. [91] have demonstrated the use of a ligand exchange method using *meso*-2,3-dimercaptosuccinic acid (DMSA). The DMSA first forms a stable coating through its carboxylic chelate bonding, and further stabilization is attained through the formation of disulfide cross-linkages between the ligands. The remaining free thiol groups are used for the attachment of target-specific antibodies. They have reported conjugation of water soluble SPIOs with a cancer-targeting antibody such as Herceptin® which specifically binds to the HER2/neu marker overexpressed in breast and ovarian cancer. Caruso et al. [58] demonstrated the transfer of various metallic nanoparticles from toluene to water using 4-(dimethyl-amino) pyridine (DMAP).

Wang reported the design and synthesis of hydrophilic organic dendron ligands for stabilizing high-quality nanocrystals in aqueous solutions. Oleic acid-stabilized monodispersed nanoparticles of Fe oxides were surface modified through the formation of an inclusion complex between surface-bound surfactant molecules and α-cyclodextrin (α-CD). After the modification, the nanoparticles can be transferred from hydrophobic solvents, such as hexane, to α-CD aqueous phase. Their efficiency depends on the initial α-CD concentration [196].

20.4.1.2 Polymeric Stabilizers

Several synthetic and natural polymers such as dextran, polyethylene glycols (PEGs), and polyvinylpyrrolidone are known to be biocompatible and promote monodispersity of SPIOs in aqueous medium (Table 20.1). Hasegawa and Hokkoku

proposed a typical manufacturing method for magnetic iron oxide particles coated with alkali-treated dextran [73]. Their method has been improved and technically modified. Many coating materials have been proposed, such as dextran, starch, arabinogalactan, glycosaminoglycan, and carboxydextran. Dextran-coated commercial products include Feridex®/Endorem®, Combidex®/Sinerem®, MION, and CLIO [35, 43, 111]. The presence of aminated dextran on the surface provides a platform for further chemical manipulations.

Surface stabilization with PEG derivatives significantly increases blood circulation time by preventing opsonization and thus avoids MPS uptake [35, 43, 111]. Additional advantages include easy excretion by the kidney; nonimmunogenic and nonantigenic properties. Nonionic block copolymer composed of PEO–PPO–PEO, such as poloxamers, has received attention due to low toxicity, non-irritation, and good performance in emulsification [143]. When the nanoparticles are stabilized with poloxamer in the aqueous phase, the PEO segment forms a "hairy" structure that cloaks the modified nanoparticles from the immune systems.

Muhammed et al. [143] reported the use of Pluronic F127 (PF127) – an ABA – type triblock copolymer consisting of poly(propylene oxide) (PPO) and poly(ethylene oxide) (PEO) to transfer the hydrophobic SPIOs coated with oleic acid to water. The PPO block associates with the alkyl tail of the oleic acid through hydrophobic interactions, while the two appending PEO chains solubilize the particles in aqueous medium. Recently, Lee et al. [112] reported the fabrication of thermal cross-linked SPION (TCL-SPION), using Si-OH containing copolymer. The carboxyl TCL-SPION was converted to an amine-modified SPION and finally to Cy5.5 TCL-SPION which even in the absence of any targeting ligand could be used efficiently in dual in vivo cancer imaging. Pellegrino et al. [140] developed a general methodology by decorating hydrophobic nanocrystals with a hydrophilic polymer shell by exploiting the nonspecific hydrophobic interactions between the alkyl chains of poly(maleic anhydride alt-1-tetradecene) and the nanocrystal surfactant molecules. Addition of bis(6-aminohexyl)amine results in the cross-linking of the polymer chains around each nanoparticles.

Our group has recently reported the use of lipid and polymeric micelles to solubilize SPIOs in water. The lipid micelles from 1,2-distearoyl-*sn*-glycero-3-phosphoethanolamine-*N*-[methoxy(polyethylene glycol)] (DSPE-PEG) lipids formed single SPIO-loaded micelles. The polymeric poly(ε-caprolactone)-*b*-poly(ethylene glycol) (PCL-*b*-PEG) copolymers resulted in clustered SPIO nanoparticles [1].

20.4.2 Inorganic Molecules

Metal core shell type SPIOs with inner iron oxide core and outer metallic shell of inorganic materials have been investigated by a growing number of researchers. Typical shell materials include silica, gold, and graphite. Silica-based core-shell nanoarchitectures composed of magnetic iron oxide cores and amorphous silica

shells are typically synthesized through a sol–gel approach. A good control of the silica shell thickness (10–100 nm) can be achieved by adjusting the silane concentration. A significant advantage of the silica shell is related to the use of well-known conjugation chemistry that allows covalent bonding of various chemical or biological species onto the silica surface. Arruebo et al. [19] proved this concept by covalent coupling of the anti-human chorionic gonadotropin (anti-hCG) antibody to the silica shell of the superparamagnetic nanoparticles, yielding potential targeted contrast agents for MRI. Zhang et al. [211] synthesized USPIO particles with silica and alkoxysilane coatings that showed high T_2 relaxivities, and were intensely internalized in immortalized progenitor cells, making them suitable for MR cell-labeling and cell-tracking experiments.

Cheon et al. [113] reported the development of the next-generation nanoprobes by fusing multiple fluorescent dyes and multiple magnetic nanoparticles into a single nanoprobe that provides superior fluorescence and MR imaging capabilities through the synergistic enhancement of its respective components. "Core-satellite" structured dual functional nanoparticles comprised of a dye-doped silica "core" (rhodamine-dye-doped silica) and multiple "satellites" of magnetic nanoparticles (Fe_3O_4) were synthesized and their utilization demonstrated as simultaneous optical and MR imaging of neuroblastoma cells expressing polysialic acids (PSAs).

One of the major challenges of use of magnetic nanoparticles in biomedical applications is the lack of surface tunability. Coating the magnetic particles with an Au shell provides an intriguing class of biomaterials to overcome such an obstacle. Because of the well-established Au–S surface chemistry and biological reactivity, Au can impart the magnetic particles with the desired chemical and/or biomedical properties. The coating also renders the magnetic nanoparticles with plasmonic properties. This makes the core/shell composite nanoparticles extremely interesting for magnetic, optical, and biomedical applications. Sun et al. [209] have synthesized core/shell structured Fe_3O_4/Au and Fe_3O_4/Au/Ag nanoparticles in aqueous solution and room temperature reaction conditions. The control on shell thickness allows the tuning of plasmonic properties of the core/shell nanoparticles to be either red-shifted (to 560 nm) or blue-shifted (to 501 nm). Zhong also demonstrated that the magnetically active iron oxide core and thiolate-active Au shell is a viable candidate for exploiting the Au surface protein-binding reactivity for bioassay and the iron oxide core magnetism for magnetic bioseparation [137]. Choa reported the synthesis of Au/Fe_3O_4 nanocomposite and the immobilization of glutathione (GSH) onto the Au/Fe_3O_4 nanocomposite thus demonstrating the possibility of using these nanoparticles in applications involving the separation and purification of biomolecules [102].

Dai and coworkers reported a novel use of a single graphitic shell coating of FeCo magnetic nanoparticles synthesized using chemical vapor deposition method nanocrystals [164]. The nanocrystals exhibit ultra-high saturation magnetization, r_1 and r_2 relaxivities, and high optical absorbance from the graphitic shell in the near-infrared region. Mesenchymal stem cells are able to internalize these nanoparticles, showing high negative-contrast enhancement in MRI.

20.5 Pharmacokinetics and Toxicology

Pharmacokinetics (absorption, distribution, metabolism, excretion) and toxicity (acute and chronic, mutagenicity) of SPIO are dependent on a number of factors including concentration (dose), hydrodynamic diameter, coating agent, charge, and method of delivery. Size differences are reflected not only in MR relaxivity differences (ratio of r_2/r_1) but also by significant differences in blood half life and distribution. As described earlier, SPIO can be coated with a myriad of surface coatings, all affecting their characteristics and distribution.

Ideal SPIO contrast agents have diameters no larger than 200 nm (SPIO plus biodegradable coating) because this prolongs blood half life and extends the particle circulation times from minutes to hours allowing SPIO to accumulate or target a site before being cleared by the body [64, 170, 202, 212]. The blood half life of all iron oxide nanoparticles is dependent on dose as well as on their hydrodynamic volume. Blood half life of SPIO nanoparticles administered to patients can vary from minutes to greater than 24 h, depending on particle size (Table 20.1) [43]. The spleen (sinusoidal lining cells) filters particles greater than 200 nm in diameter including SPIOs. Below 5–6 nm, particles are rapidly removed by extravasation and renal clearance [41]. When comparing the SPIO with the same coating material, USPIO is less prone to liver uptake as opposed to SPIO due to their small size (e.g., ferumoxtran-10 vs. ferumoxides and SHU 555 C vs. SHU 555 A).

To date, studies have shown that iron oxide nanoparticles are nontoxic and have minimal impact on cell viability and function [7, 14, 16, 17, 43, 66, 70, 125, 135, 145, 171]. SPIOs share their specific uptake by macrophages through phagocytosis. In a study by Metz et al. [127], the capacity of human monocytes to phagocytose SPIO (Ferucarbotran) and USPIO (SHU 555 C) at different concentrations and incubation times was evaluated. The results showed no loss in cell viability and confirm spontaneous uptake of particulate contrast agent by a macrophage cell line. Monocytes are capable of ingesting large quantities of particulate SPIO by phagocytosis, with subsequent compartmentalization in secondary lysosomes within the cytoplasm. As opposed to other, non-phagocytic cells such as lymphocytes, monocytes do not need the aid of transfection agents for iron oxide internalization. A maximum iron oxide uptake up to 50 pg Fe/cell was measured without impairment of cell viability. In a different study [161], SPIO distribution and elimination were evaluated by double-labeling using ^{14}C and ^{59}Fe ferumoxtran-10 nanoparticles. In the end, it was shown ferumoxtran-10 is completely degraded in the macrophage lysosomal compartment within 7 days. After uptake by the macrophages, the dextran coating undergoes progressive degradation by intracellular dextranases and is almost exclusively eliminated in the urine (89% in 56 days). The iron contained in ferumoxtran-10 is incorporated into the body's iron stores and is progressively found in the red blood cells. Like endogenous iron, the radiolabeled ^{59}Fe is very slowly eliminated from the body. Similar rates of erythrocyte incorporation have been reported for radiolabeled ferritin, the physiological storage form of iron. In addition, similar behavior has also been described for ferumoxides [198]. Dextran-coated CLIO nanoparticles showed that iron incorporation did not affect cell viability,

differentiation, or proliferation of human hematopoietic cells [119]. Similarly, the influence of PEG-modified SPIO nanoparticles on human fibroblasts was studied [65]. The PEG-coated nanoparticles did not affect the cell adhesion behavior or morphology. In general, iron oxide nanoparticles coated in biodegradable coating appear to have no long-term toxicity and are safe for use.

In animal trials, pharmacokinetics and toxicology of AMI-25 (Endorem®/ Feridex®) were evaluated by ^{59}Fe radiotracer in Sprague-Dawley rats and beagle dogs [197]. One hour after administration of AMI-25 to rats (18 μmol Fe/kg; 1 mg Fe/kg), 82.6% of the administered dose was sequestered in the liver and 6.2% in the spleen. Peak concentrations of the ^{59}Fe radiotracer were found in the liver after 2 h and in the spleen after 4 h. ^{59}Fe slowly cleared from the liver (half life, 3 days) and the spleen (half life, 4 days). The iron was incorporated into hemoglobin of erythrocytes in a time-dependent fashion. Only minimal amounts of ^{59}Fe were detected in other tissue, such as the kidney, lung, and brain. The whole body clearance of ^{59}Fe was 20% after 14 days and 35% after 28 days with an extrapolated half life of whole body clearance of 45 days. Studies on acute toxicity revealed that AMI-25 had no lethal effect on the animals at the highest dose injected (3,000 μmol Fe/kg), 150 times the dose proposed for MR imaging of the liver. Subacute toxicity studies revealed no effect on mortality, morbidity, body weight, or food consumption. The final conclusion was that AMI-25 is a fully biocompatible contrast agent.

Human clinical trials with AMI-25 were performed by Berlex Laboratories [25]. In this study, AMI-25 was administered to three, healthy adult male volunteers (dose = 0.56 mg/kg diluted in 100 mL of 5% dextrose and intravenously infused over 30 min). Bolus injections are usually not administered because of cardiovascular side effects and lumbar pain. For example, the amount of iron in a single dose is calculated to be 39.2 mg of iron for a 70 kg individual. This equates to less than 1/5 the amount of iron contained in one whole unit of blood. Normal liver contains approximately 0.2 mg of iron per gram, and total human iron stores amount to 3,500 mg. The total amount of iron oxide necessary for diagnostic imaging is small compared to the body's normal iron store. Chronic iron toxicity develops only after the liver iron concentration exceeds 4 mg of iron per gram [30]. Hypoglycemia may accompany liver dysfunction. Peak serum iron concentration was 5.5 μg/mL and AMI-25 was completely cleared from the blood by 25 h after administration (half life 2.4 ± 0.2 h). At 24 h, serum iron increased, and the percent saturation of iron-binding capacity decreased in a dose-dependent fashion. By 7 days, serum iron returned to pre-administration levels, and serum ferritin increased. These results are consistent with the iron in AMI-25 entering the usual iron metabolism cycle. MR imaging results showed no difference in loss of signal intensity on images obtained between 0 and 3.5 h after infusion indicating a wide scan window for imaging. Unfortunately, acute severe back, leg, or groin pain occurred in some patients. In clinical trials, 2.5% (55/2240) of the patients experienced pain severe enough to cause interruption or discontinuation of the infusion. In most patients, the symptoms developed within 1–15 min (and lasted up to 45 min). Most other adverse reactions were mild to moderate, of short duration, and resolved spontaneously without treatment. However, in a few cases, anaphylactic-like reactions and

Table 20.1 Physical properties of iron oxides commercially available or under clinical investigation

Names	Coating	Hydrodynamic diameter[a] (nm)	Human blood half life (h)	r_2, relaxivity ($mM^{-1}s^{-1}$)	r_2/r_1	References
Ferumoxsil AMI-121 Lumirem® Gastromark®	Silicon	300	Oral	72 (0.47 T)[b]	22.5	[70, 92]
Ferumoxide AMI-25 Feridex® Endorem®	Dextran T10	80–150	Biexponential: 0.1–0.33, 2–3	107 (0.47 T)[b] 152 (0.47 T)[c] 41 (1.5 T)[c]	4.5 5.6 8.7	[92, 156, 169, 197]
Ferucarbotran SHU-555A Resovist®	Carboxydextran	62	Biexponential: 0.065–0.1, 2.4–3.6	151 185.8	5.9 9.6	[150, 195]
Ferumoxytol AMI-7228	Carboxydextran	28–32	10–14	83 (0.47 T)[b]	2.2	[167]
Ferumoxtran AMI-227 BMS 180549 Sinerem® Combidex®	Dextran T10, T1	15–30	>24	44.1 (0.47 T) 53.1 (0.47 T)[b]	2.0 2.3	[92, 126, 198]
SHU-555C Supravist®	Carboxydextran	20	6	60 (0.47 T)[d]	2.5	[167]
NC100150 Feruglose Clariscan®	Pegylated starch	11–15	4	36 (1.4 T)[c]	2.3	[29, 44]

[a] dynamic light scattering
[b] 0.5% agar, 39°C
[c] water, 37°C
[d] plasma, 40°C

hypotension have been noted in some patients receiving AMI-25 or other iron and dextran-containing formulations [8, 25, 54, 216]. In clinical trials, anaphylactic and allergic adverse events occurred in 0.5% (11/2240) of the patients who received Feridex®. These events include dyspnea, other respiratory symptoms, angioedema, generalized urticaria, and hypotension all requiring treatment.

20.6 Biomedical Applications of Magnetic Nanoparticles

20.6.1 Magnetic Resonance Imaging

Since the advent of MRI, there has been rapid development and study of magnetic nanoparticles for use in the biomedical field. MRI is based on a physics phenomenon called nuclear magnetic resonance discovered in the 1930s by Bloch and Purcell (Nobel Prize in Physics 1952), where the magnetic properties of atomic nuclei are investigated. In 1971, Damadian discovered the basis for using magnetic resonance imaging as a tool for medical diagnosis. He found that different kinds of animal tissue emit response signals with varying length, and that cancerous tissue emits response signals that last much longer than non-cancerous tissue [45]. The world's first patent issued in the field of MRI was granted to Damadian in 1974 [46]. In 2003, the Nobel Prize in Medicine was awarded to Lauterbur and Mansfield for their discoveries concerning MRI.

MRI provides excellent in vivo imaging capability with high spatial (<1 mm) and temporal resolution, excellent soft tissue contrast, and sensitivity to blood flow. However, the primary limitation of MRI has been its low sensitivity. In order to overcome this disadvantage, signal amplification strategies, such as the use of contrast agents, are employed to provide greater signal intensity that generates higher contrast from the surrounding tissue. Of particular interest are magnetic particles, specifically, SPIO nanoparticles, consisting of maghemite (γ-Fe_2O_3), magnetite (Fe_3O_4), and other metal ferrites. These contrast agents are extremely strong enhancers of transverse proton relaxation.

20.6.1.1 Anatomical Imaging

Gastrointestinal Tract Imaging

One of the first applications for SPIO nanoparticles was as an oral contrast agent used to image the gastrointestinal (GI) tract [43, 70, 195]. In MRI as well as computed tomography (CT), it is necessary to increase the contrast between the GI tract and the surrounding organs with negative contrast agents being better suited for these types of applications. Oral SPIO contrast formulations are usually composed of larger SPIO particles coated with a non-biodegradable, insoluble matrix and suspended in viscosity-increasing agents (usually based on ordinary food additives, such as starch and cellulose) [23, 70]. These formulations prevent the ingested iron from being absorbed and metabolized by the body and to improve homogenous

contrast distribution throughout the bowel. If SPIO do aggregate, magnetic susceptibility artifacts may result, especially at high field and when gradient echo pulse sequences are used [32].

A first agent, ferumoxsils are composed of approximately 10 nm nanoparticles coated by a layer of inert silicon with a hydrodynamic diameter of 300 nm. Ferumoxsils are also know as AMI-121 or have trade names "Gastromark®" and "Lumirem®," manufactured by Advanced Magnetics (US) and Guerbet (EU), respectively. The reported T_2 and T_1 relaxivity for AMI-121 are 72 and 3.2 $mM^{-1}s^{-1}$, respectively [70, 92]. A second agent, oral magnetic particles (OMP), trade name "Abdoscan®" manufactured by Nycomed (EU), are composed of polystyrene-coated (ferristene) particles below 50 nm with a total particle size of 3.5 μm [23, 24, 85, 124, 189]. The OMP concentration typically used is 0.5 g/L with the particles containing 25% (w/w) SPIO. Oral SPIO are normally administered over a 30–60 min period, with a volume of 400 mL for upper abdomen imaging, and 900 mL for contrast enhancement of the whole abdomen. Figure 20.3 illustrates the proton density images of the rat abdomen before and after the oral administration of OMP agents. Significant image darkening was observed after OMP ingestion, leading to clear demarcation of the stomach in the axial images. Generally, GI contrast agents are well tolerated, with mild side effects, such as nausea and vomiting occurring in 1–5% of patients [110].

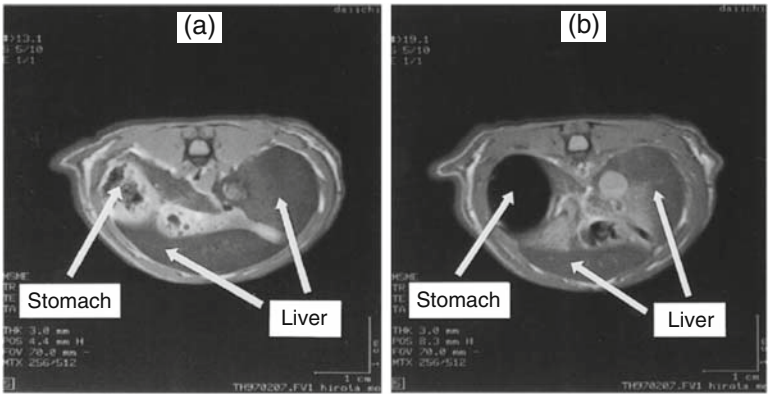

Fig. 20.3 Proton density-weighted MR imaging of rat abdomen: (**a**) no administration and (**b**) administration of the suspension of fast dispersible OMP granules, 4 mL/rat. Copyright © (1998) *Elsevier. All rights reserved*

Liver and Spleen Imaging

In addition to GI tract imaging, SPIOs are frequently used in hepatic imaging. After intravenous injection, SPIOs are nonspecifically taken up by the reticuloendothelial system (RES) of the liver and spleen. With T_2-weighted ($T_{2\text{-w}}$) sequences, the presence of SPIO nanoparticles decreases signal intensity of normal parenchyma of liver

and spleen. For example, Kupffer cells are located exclusively in healthy liver tissue. The absence of these cells in malignancies can be exploited to discriminate between healthy and diseased tissues through SPIO-enhanced contrast [43]. Tumors have a lesser decrease in signal intensity after SPIO administration because they lack these macrophages. Liver tumors or metastases as small as 2–3 mm can be detected [43]. In addition to detection and characterization of liver lesions, SPIOs have also been shown capable of detecting focal splenic tumors. The use of SPIO increases both lesion conspicuousness and lesion detection compared to non-enhanced imaging [163].

The first contrast agents to be developed and marketed for this purpose were ferumoxides. Ferumoxides are also known as AMI-25, trade names "Feridex®" and "Endorem®" manufactured by Advanced Magnetics (US) and Guerbet (EU), respectively. They consist of a T10-dextran-coated particle with a hydrodynamic diameter of 120–180 nm (particle and crystal size approximately 15 and 5 nm, respectively) [43]. The reported T_2 and T_1 relaxivity range from 107 to 152 and 23.7–27.0 $mM^{-1}s^{-1}$, respectively [92, 156]. The recommended mode of administration is a biphasic infusion (2 mL/min over 10 min and 4 mL/min over 20 min) of a dose of 15 μmol Fe/kg in 100 mL of 5% glucose [197]. AMI-25 allows a wide window for T_2 and ${T_2}^*{}_{-w}$ imaging of 0.5 to 6 h after administration [149]. AMI-25 effectively accumulates in the liver (approximately 80% of the injected dose) and spleen (5–10% of the injected dose) within minutes of administration; blood half life is 6 min (see Table 20.1) [197]. Similarly, ferucarbotran is a SSPIO characterized by a carboxydextran coating. Ferucarbotran is also known as SHU 555A or trade name "Resovist®" manufactured by Schering AG (EU). The crystal of SHU 555A is 4.2 nm, and the hydrodynamic diameter is 62 nm. The reported T_2 and T_1 relaxivities range from 151.0 to 185.8 and 19.4–25.4 $mM^{-1}s^{-1}$, respectively [150, 195]. A dose of 8 μmol Fe/kg is the recommended quantity for T_{2-w} imaging. Due to its smaller size and thus stronger T_1 effect, SHU 555A has also been used for T_{1-w} imaging and MR angiography.

Numerous preclinical and clinical trials have been carried out to demonstrate SPIO efficacy in detection of focal lesions in both the liver and the spleen [60, 71, 94, 98, 99, 106]. Arbab et al. [13] investigated whether ferumoxide-enhanced T_{2-w} MR images alone can allow for differentiation of metastases from benign lesions in the non-cirrhotic liver. In this study, 60 lesions (22 metastases, 20 hemangiomas, and 18 cysts) were identified in 42 patients, and fast spin-echo T_{2-w} MR images were obtained before and after administration of ferumoxides. Ferumoxides-enhanced images showed significantly higher diagnostic accuracy than that of unenhanced images and concluded ferumoxides-enhanced T_{2-w} MR images appear useful in differentiating metastases from benign, nonsolid lesions in the liver. Namkung et al. [131] evaluated the efficacy of ferucarbotran for characterizing focal liver lesions. In this study, 68 patients with 46 malignant and 22 benign focal liver lesions were evaluated. The group concluded that the percentage of signal intensity loss due to the nonspecific uptake of SPIO can be an accurate tool for characterizing benign and malignant lesions. Finally, Kim et al. [103] compared the diagnostic performance of gadobenate dimeglumine (Gd-BOPTA)-enhanced MR imaging vs. SPIO-enhanced

imaging for detection of liver metastases. Twenty-three patients with 59 liver metastases underwent Gd-BOPTA- and SPIO-enhanced MR imaging on a 1.5 T unit. Figure 20.4 shows the dramatic difference in detecting these types of liver metastases. With Gd-BOPTA-enhanced imaging, only two low intensity liver masses were visible. In the opposite image, SPIO-enhanced imaging clearly shows the branched structure of the liver. Within the same image, the two larger masses as well as a smaller mass are easily identified.

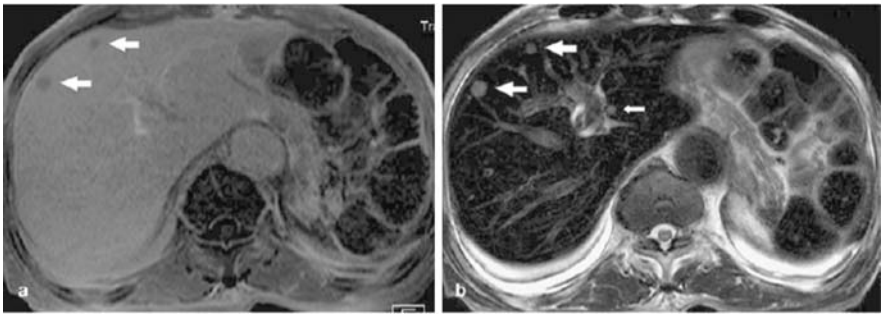

Fig. 20.4 Multiple liver metastases in a 48-year-old man with gastric carcinoma: (**a**) gadobenate dimeglumine-enhanced 1-h delayed phase MR image shows two low signal intensity liver masses (*arrows*), (**b**) superparamagnetic iron oxide-enhanced respiratory-triggered T_2-weighted turbo spin echo image shows another tiny high signal intensity mass (*small arrow*) as well as two masses (*large arrows*) in the right lobe of the liver.

Lymph Node Imaging

Nodal disease is an independent, adverse prognostic factor in many types of cancers. However, diagnostic imaging of lymph node metastases is difficult because signal intensities of metastatic nodes differ from those of normal nodes only in size. This poor preoperative staging can then influence the oncologist's decision to use neoadjuvant therapy or the surgeon's decision to perform nodal dissection [105]. SPIOs which can be taken up by normal nodes following intravenous or subcutaneous injection have made differentiation possible. Specifically, the SPIO extravasate from the vasculature to the interstitial space, where they are transported to the lymph nodes via the lymphatic vessels. Hence, metastatic nodes can be differentiated from normal nodes based on the absence of signal intensity change between pre- and post-contrast scans [11, 12, 72, 195].

In contrast to SSPIO, smaller iron oxide nanoparticles are found to accumulate in the lymph nodes. The first agent and most widely studied is ferumoxtran-10. Ferumoxtran-10 is characterized as an USPIO and is also known as AMI-227, trade names "Combidex®" and "Sinerem®" manufactured by Advanced Magnetics (US) and Guerbet (EU), respectively. The iron oxide core is approximately 5 nm surrounded by an 8–12 nm layer of T10 dextran coating resulting in a final size of

less than 30 nm. The reported T_2 and T_1 relaxivity for the USPIO are 44.1–53.1 and 21.6–22.7 $mM^{-1}s^{-1}$, respectively [92, 198]. After administration, the USPIO is taken up by macrophages within the lymph nodes, appearing dark on the MR images. In contrast, metastatic nodes that are partially or completely replaced by tumor cells do not possess the same levels of phagocytotic activity as normal nodes and maintain the same signal intensity on post-contrast MR images as shown in Figure 20.5. In this study by Harisinghani et al. [72], MRI was performed on 80 patients with pre-surgical clinical stage T1, T2, and T3 prostate cancer who underwent lymph node resection or biopsy. MRI was performed pre- and 24 h post-intravenous injection of 2.6 mg/kg of ferumoxtran-10. Sixty-three lymph nodes from 33 patients had histopathological detected metastases. Of these, 45 (71.4%) did not fulfill the imaging criteria for malignancy. However, ferumoxtran-1-enhanced MRI was able to correctly identify all patients with nodal metastases. Nodal metastatic infiltration measuring 5–10 nm was identified. Anzai et al. [10] investigated the efficiency of MR imaging with dextran-coated USPIO to distinguish metastatic and benign nodes in patients with head and neck cancer. In this study involving 12 patients, 40 out of 42 histologically proven metastatic nodes and 41 out of 49 benign nodes were detected, yielding a 95% sensitivity and 84% specificity for diagnosis of tumor-bearing lymph nodes. In a comparative study, 16 patients with esophageal cancer underwent MRI scanning before and 24 h after intravenous administration

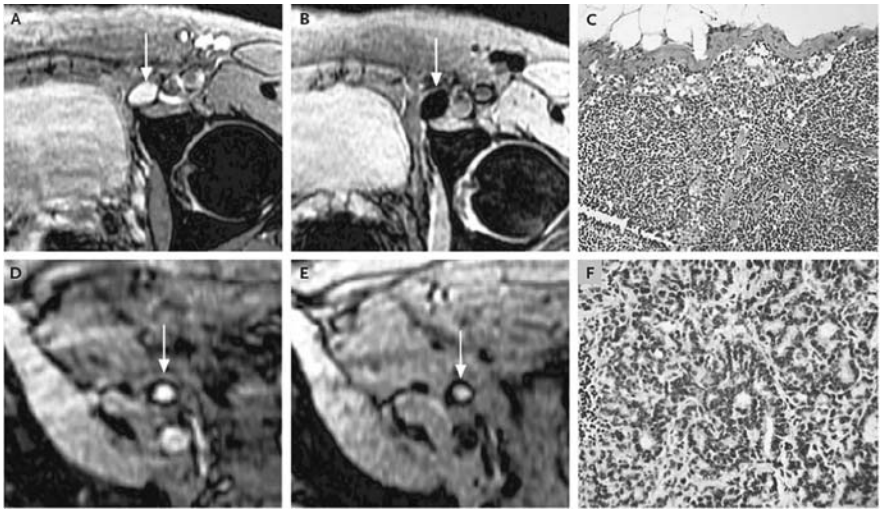

Fig. 20.5 MRI nodal abnormalities in patients with prostate cancer: (**A**) conventional MRI of normal lymph node, (**B**) MRI of a normal lymph node obtained 24 h after IV administration shows accumulation of lymphotropic SPIO, (**C**) corresponding histology (hematoxylin and eosin, 125X), (**D**) conventional MRI shows a high signal intensity in an enlarged iliac node completely replaced by tumor, (**E**) nodal signal intensity remains high after SPIO administration, and (**F**) corresponding histology (hematoxylin and eosin, 200X).

of ferumoxtran-10 [134]. Of the 408 resected lymph nodes, imaging results of 133 nodes could be compared with histopathologic findings. Twenty-four lymph nodes had histopathologic metastases. Using their enhancement criteria, sensitivity was 100%, specificity was 95.4%, and accuracy was 96.2% for the diagnosis of metastatic nodes. Therefore, without SPIO-enhanced MRI, metastatic lymph nodes in these studies would have been missed had size criteria alone been used.

20.6.1.2 Molecular Imaging and Targeting

Molecular imaging can be broadly defined as the "non-invasive and repetitive imaging of targeted macromolecules and biological processes in living organisms" [35]. Molecular imaging using MRI requires the use of ligands (e.g., antibodies, proteins, peptides) for selective binding to targeted disease markers. These ligands, in turn, need to be conjugated to MR contrast agents in order to induce a contrast difference from non-targeted tissue. In this way, anatomical information on MR images can be discerned or marked in order to detect diseases, such as cancer, at its earliest stage. Numerous examples demonstrate the potential application of SPIO for molecular imaging.

As a typical example, targeting agents such as proteins are coupled to insoluble polysaccharides using simple conjugation methods. Periodate oxidation/borohydride reduction is used to produce reactive aldehyde groups on the nanoparticle's surface, which will react with amino groups on the proteins (e.g., HSA or transferrin attachment to carboxydextran nanoparticle or a monoclonal antibody (mAb) or wheat germ agglutinin lectin on a dextran nanoparticle) [51, 108, 151, 158, 201]. Using this method, antimyosin Fab ($R_{11}D_{10}$) was attached to MIONs for immunospecific MR imaging of myocardiac infarction [201], to intact mAbs for immunospecific detection of intracranial small cell lung carcinoma [151], as well as to human polyclonal immunoglobulin (IgG) for the detection of induced inflammation [200], and to synaptotagmin I for detection of apoptotic tumor cells [214]. However, in the case of the transferrin receptor, a substantial loss of the protein biological activity was observed [159]. To minimize this type of detrimental effect, new non-oxidative chemistry was developed. For example, a dextran-coated nanoparticle is cross-linked by epichlorohydrin and ammonia resulting in an amine-terminated CLIO nanoparticle capable of conjugating biovectors with a vast range of heterobifunctional linkers [207]. Weissleder's group has used this strategy to graft transferrin, annexin, V, anti-VCAM, or anti-E-Selectin antibodies, oligonucleotides, and TAT peptides to CLIO nanoparticles [77, 89, 96, 142, 215]. This technology platform was subsequently used to develop a wide nanoparticle library consisting of 146 nanoparticles decorated with different synthetic small ligands that recognizes apoptotic cells [160, 204].

Alternate methods to attach mAbs to magnetic nanoparticles include glutaraldehyde cross-linking chemistry [152], biotin streptavidin system [20, 21, 36], amine-sulfhydryl group linkage [180, 181], and disulfide chemistry [53, 155]. Specific examples of some proteins/peptides used for MR visualization include cholecystokinin- [148] and secretin-linked [166] nanoparticles used for their

respective pancreatic receptor and may aid in the diagnosis of pancreatic cancer. Transferrin-SPIO nanoparticles have been used for specific labeling and detection of gliosarcoma [82, 128, 203] and breast carcinoma [108], with and without transfection of the transferrin receptor encoding gene, respectfully. Finally, targeting of beta-amyloid plaques in a transgenic mouse model of Alzheimer's disease has resulted in specific enhancement of lesions on the ex vivo images. Specific plaque enhancement was obtained in vivo using MIONs labeled with Abeltal-40 peptide [190]. Table 20.2 shows current examples of targeted MR contrast agents in molecular imaging applications.

20.6.1.3 Cellular Imaging and Tracking

Similar to molecular imaging, a promising new direction for SPIO is their use in tracking the distribution of cells in vivo [35, 43, 179]. MR cell tracking, with its excellent spatial resolution, can be used as a noninvasive tool to provide unique information on the dynamics of cell movements. These studies usually involve implanting SPIO-loaded cells into living subjects, tracking their movement in the body, and/or localization in specific tissues. Alternately, cellular imaging in the future could be applied to monitor cell therapy in patients. Currently, SPIOs are the MR contrast agent of choice for cell labeling due to their biocompatibility and strong T_2 effect. Various strategies have been developed to efficiently load cultured cells with sufficient quantities of SPIO to ensure enough contrast for in vivo imaging.

Within the MR cellular imaging field, a major focus of study is stem cells, given their remarkable potential to develop into many different cell types within the body. But before their therapeutic possibilities can be exploited, the dynamics of cell migration and differentiation after implantation into the host organ must be studied. MR tracking may serve in experimental animal models to study how lesions and stimuli target cell migration, at what speed cells migrate, and for how long they persist at the target site. For example, visualizing transplanted cells in experimental central nervous system (CNS) diseases has yielded good examples for such use of this tool. Oligodendrocyte progenitors were magnetically labeled using anti-Tfr mAbs and transplanted into the spinal cord of 7-day old myelin-deficient rats [34]. Ten to fourteen days later, the spinal cords were removed and imaged at 4.7 T at 78 μm resolution. Migration of labeled cells was easily identified on MR images as streaks of hypointensity, primarily along the dorsal column, over a distance of up to 10 mm away from the injection site. This study showed that magnetically labeled oligodendrocyte progenitor cells responded adequately to the normal development signals in the post-natal myelinating CNS and retained their capacity to myelinate axons in vivo. Neural stem cell transplantation has been shown to attenuate the severity of experimental autoimmune encephalomyelitis (EAE), an animal model of multiple sclerosis. Using magnetically labeled mouse neurospheres and human embryonic stem cell (hESC)-derived neurospheres, serial MRI was used to assess the biodynamics of transplanted cell migration in a chronic mouse EAE model [28]. Magnetic labeling did not affect the in vitro and in vivo characteristics of cells as

Table 20.2 Targeted superparamagnetic iron oxide nanoparticles for molecular imaging

Targeted contrast media	Experimental conditions	Ligand	Biological target	Result	References
MION-IgG	In vivo	Ab	Inflammation	Accumulation at inflammation site and confirmed with histology.	[200]
USPIO-AG	In vitro, in vivo	Arabinogalactan	Asialoglycoprotein receptors on hepatocytes	Due to lack of ASG receptors in primary tumors, high tumor-liver contrast possible.	[146, 147, 199]
USPIO-RGD	In vitro, in vivo, ex vivo	c-RGD peptide	Thrombus imaging	USPIO–RGD resulted in better thrombus visualization than control ex vivo and maximum enhancement post ~ 1 h.	[88]
CLIO-Cy5.5-annexin V	In vitro	Dye-annexin	Jurkat T cells	Bimodal approach to recognize normal and apoptotic cells.	[160]
SPIO-PEG-folate	In vitro	Folic acid	Breast cancer cells	SPIO–PEG–FA internalized into BT-20 cancer cells and show higher cellular uptake compared to PEG or folate alone.	[213]
CLIO-transferrin	In vitro	Glycoprotein	Gliosarcoma	Successful development of high throughput screening and detection of cellular uptake.	[77]
USPIO-transferrin	In vivo	Glycoprotein	Mammary carcinoma	Showed a signal reduction (25–55%) 150 min post-injection.	[108]
USPIO-transferrin	In vitro, in vivo	Glycoprotein	Tf receptors	Imaging of gene expression.	[82, 108, 128, 203]
CLIO-F(ab′)$_2$ (anti-human E-selectin)	In vitro	mAb	E-selectin	Showed a highly specific T_2 weighted signal darkening associated with treated endothelial cells.	[96]
MION-antiHer-2/*neu*	In vitro	mAb	Melanoma and mammary cell lines	Receptor-specific T_2 contrast change on Her-2/*neu* positive tumor cells.	[56]
MION-L6 antibody	In vivo	mAb	Surface antigen on human carcinoma	Specific pattern enhancement in LX-1 intracranial tumors 6 h post-injection.	[151]
SPIO-528	In vitro, in vivo	mAb	EGFR	Immunoreactivity is preserved with specific binding to squamous cell carcinoma of the oesophagus.	[175]
SPIO-A7	In vitro, in vivo	mAb	Colorectal carcinoma	Significant in vivo tumor accumulation of targeted SPIO as compared to the control group.	[182]

Table 20.2 (continued)

Targeted contrast media	Experimental conditions	Ligand	Biological target	Result	References
SPIO-antibody	In vitro, in vivo	mAb	Surface antigen on neuroblastoma	Specific binding of these particles is demonstrated.	[152]
SPIO-antiCD4$^+$, -antiCD8$^+$	In vivo	mAb	T cells	Monitored the infiltration of T cells in the CNS over time in infected animals.	[142]
SPIO-antiCEA	In vitro, in vivo	mAb	Carcinoembryonic antigen (CEA)	Peptide carrier for magnetite showed very good in vitro characteristics but caused severe in vivo problems.	[180, 181]
SPIO-antiHer-2/*neu*	In vitro, in vivo	mAb	Breast cancer cells	Enhanced T_2 and $T_2{}^*$ images at 9.4 T for pre-labeled mAb-biotin tumor cells followed by incubation with labeled-SPIO demonstrated with positive controls.	[20, 21]
SPIO-antilymphocyte	In vitro	mAb	Lymphocyte	Biotinylated-SPIO + labeled biotinylated anti-lymphocyte-mAb + streptavidin gave strong and selective negative contrast enhancement of suspensions at 2.0 T.	[36]
USPIO-610	In vitro, in vivo	mAb	Surface antigen on colon carcinoma	Immunoreactivity is preserved with specific tumor binding.	[39]
USPIO-antimyosin	Ex vivo	mAb	Myocardial infarction	Marked decrease in signal intensity of infarcted myocardium 1 h post IV.	[201]
CLIO-EPPT	In vitro, in vivo	Peptide	uMUC-1	Specific accumulation of the probe in uMUC-1-positive tumors and virtually no signal in control tumors.	[129]
CLIO-TAT	In vitro	Peptide	Hematopoietic C34+ cells	Internalization into hematopoietic cells without toxicity.	[119]
CLIO-TAT peptide	In vitro	Peptide	Cellular uptake	Significant uptake of TAT-labeled CLIO.	[89, 215]
MION-Aβ1-40	In vivo	Peptide	Aβ-amyloid plaque	Intraarterial injection of magnetically labeled Aβ1-40, with mannitol to transiently open the BBB, enabled the detection of many amyloid-β plaques.	[190]
USPIO-pep(VCAM-1)	In vitro, in vivo	Peptide	VCAM-1	Binding of targeted USPIO in atherosclerotic lesions of ApoEko mice and in TNFa-inflammatory mice.	[100]
MION-20-CCK	In vitro, in vivo	Peptide hormone	Pancreas	Studies show a decrease in T_2 times in pancreatic tissue but not in tumor.	[148]
MION-46-strept-secretin	In vitro, in vivo	Peptide hormone	Pancreas	Distribution studies in rats showed a higher pancreatic accumulation as compared to the control group.	[166]
SPIO-C_2	In vitro, in vivo	Synaptotagmin I	Phosphatidylserine of apoptotic cells	Feasible to detect of apoptotic cells treated by chemotherapy.	[214]

multipotential precursors. It was also shown that cell migration occurred along white matter tracts, especially the corpus callosum, fimbria, and internal capsule predominantly early in the acute phase of disease and in an asymmetric manner. The distance of cell migration also correlated well with clinical severity of disease and the number of microglia in the white matter tracts, supporting the idea that inflammatory signals promote transplanted cell migration.

MR tracking outside the CNS has also been performed for other cell types and disease models including mesenchymal stem cells (MSCs), found in bone marrow, for cellular repair of cardiovascular and myocardial injury. The concept is that these cells can contribute to stromal support, angiogenesis, or the formation of new cardiomyocytes [35]. The goal is to non-invasively identify transplanted MSCs months post-injection and be able to correlate myocardial function and infarct size with MRI. In a swine myocardial infarction (MI) model, injected iron fluorophore-labeled MSC into normal and infarcted myocardium enabled ready detection in the beating heart on a conventional 1.5 T cardiac MR scanner after transplantation [75]. At 3 weeks, hypointense artifacts were still present and appeared to persist up to 12 weeks post-injection. In a similar swine MI model with x-ray fluoroscopic intramyocardical injection of Feridex®-PLL labeled MSCs, successful contrast-enhanced MRI and serial MSC tracking was demonstrated in two animals (5 total including control) [107]. Additional examples of MR tracking, distribution, and migration of stem cells and progenitor cells in different animal models are shown in Table 20.3.

20.6.2 Therapeutic Applications

20.6.2.1 Hyperthermia

Magnetic fluid hyperthermia is a treatment modality for the eradication of cancer tissues using an alternating magnetic field. The magnetic waves are not absorbed by living tissue and can permeate throughout the body. When subjected to a variable magnetic field, magnetic nanoparticles generate heat due to magnetic hysteresis loss. The amount of heat generated depends on the physical properties of the magnetic material and the magnetic field parameters [59, 74]. Cancer cells are destroyed at elevated temperatures (42–46°C), whereas normal cells can survive at these temperatures [33, 67, 194]. The architecture of the vasculature inside solid tumors is chaotic, resulting in regions with hypoxia and low pH, which is not found in normal tissues [187]. These environmental factors make cells more sensitive to hyperthermia. At temperatures above 42°C, the exposure time can be halved with each 1°C rise in temperature, which will result in equivalent cell death [144]. Most normal tissues, with the exception of central nervous tissue, remain undamaged by treatment for 1 h at a temperature up to 44°C [52]. For the CNS, irreversible damage was found after treatment at 42–43°C for longer than 40 to 60 min [168]. Treatment of peripheral nerve tissue for times greater than 30 min at 44°C, or equivalent

Table 20.3 Examples of magnetically labeled cells for MR cell tracking

Animal model	Stem cells	Labeled nanoparticle	Result	References
E.G7-OVA tumor bearing mice	Activated T-cells	Citrated SPIO	Tumor regression correlated with T-cell uptake.	[79]
Thrombotic stroke in rats	Bone marrow and ESC	Endorem®	Hypointense signal persisted for more than 50 days.	[86]
C57B1/6 mice injected with melanoma cell lines	CD8 + cytotoxic T lymphocytes	CLIO-HD	In vivo detection of CLIO-HD-CD8 + T cells with threshold of ~3 cell/voxel.	[104]
C-6 rat glioma tumor-bearing nude mice	$hAC133^+$ cells	Feridex® + protamine sulfate	Demonstrated incorporation of labeled cells into the neovasculature of implanted flank tumors at 7 T.	[18]
Neonatal NOD- SCID mice	hCNS-SCns	Feridex® + protamine sulfate	Transplanted hCNS-SC respond to cues characteristic for the ambient microenvironment resulting in distinct migration patterns.	[68]
Nude rats	hMSCs	Ferumoxides + poly-L-lysine	Site-specific delivery of hMSCs (liver) via magnetic targeting.	[15]
Mdx mice (muscular dystrophy)	mc13 cells	Ferumoxides + poly-L-lysine	Endosomal accumulation of SPIO resulted in 3-D, noninvasive detection of labeled cells.	[37]
Mice with muscle disorder	MD-100	SPIO	May be useful for noninvasive monitoring of stem cell transfer, replacing sequential muscle biopsies and tissue harvesting.	[191]
Myocardial infarction in mice	Mouse ESC	Ferumoxides + lipofectamin	Stem cells were observable for at least 5 weeks after injection.	[76]
CCl_4-induced hepatocyte necrosis and inflammation in rats	Rat MSCs	Endorem® + Superfect®	Signal intensity loss in renal cortex; cells were detected for up to 7 days in kidney and 12 days in liver.	[31]
Rats with acute kidney injury	Rat MSCs	Resovist®	Qualitative and quantitative in vivo cell tracking and monitoring of organ distribution feasible in MRI at 3T.	[84]
CCl_4-induced liver damage in rats	Rat bone MSCs	Fe_2O_3 + poly-L-lysine	Intrasplenic transplantation of the labeled cells could be depicted in vivo.	[90]
Sprague-Dawley rats	Rat neural stem cells	Au-MION	Grafted cells do not migrate efficiently when implanted in the intact rat spinal cord; also very few cells appeared to have survived to the 1 month time point.	[192]
Glioma-bearing SCID mice	$Sca1^+$ bone marrow cells	Feridex® + poly-L-lysine	MRI can detect incorporated labeled $Sca1^+$ cells in tumor vasculature as part of ongoing angiogenesis and neovascularization.	[9]

dose, resulted in temporary functional loss, which can be recovered within 4 weeks [206]. To this end, much work has been done in vitro and with animal experiments to manifest hyperthermia as a therapeutic modality for cancer. Significant improvement in clinical outcome has been demonstrated for tumors of the head and neck, breast, brain, bladder, cervix, rectum, lung, oesphagus, vulva and vagina, and also for melanoma [187].

In a pilot study by Johannsen et al. [87], magnetic fluid hyperthermia was evaluated as a minimally invasive technique for treatment of prostate cancer. This was the first clinical application of interstitial hyperthermia using magnetic nanoparticles in locally recurrent prostate tumors. Nanoparticle suspensions were injected transperineally into the prostate under transrectal ultrasound and fluoroscopy guidance. The nanoparticles used in this study were coated with an aminosilane-type shell in water (MagForce® MFL AS, MagForce® Nanotechnologies GmbH, Berlin, Germany) and had an average particle core size of 15 nm. Concentration of ferrites in aqueous solutions was 120 mg/mL. Using an alternating magnetic field with a frequency of 100 kHz and variable field strength (0–18 kAm^{-1}), invasive thermometry of the prostate was carried out with CT scans following treatment to monitor nanoparticle distribution and probe position. In the first patient treated, maximum and minimum intraprostatic temperatures measured at a field strength of 4.0–5.0 kAm^{-1} were 48.5°C and 40.0°C during the first treatment and 42.5 and 39.4°C during the sixth treatment, respectively. In this first clinical application of hyperthermia using magnetic nanoparticles in prostate cancer, the aims to prove feasibility as a minimally invasive technique and to obtain thermoablative temperatures in the prostate were achieved. These first clinical successes prompted phase I studies in order to further evaluate feasibility, toxicity, and quality of life during hyperthermia using magnetic nanoparticles in patients with biopsy-proven local recurrence of prostate cancer following radiotherapy with curative intent.

In many cases, hyperthermia is used in conjunction with other therapies such as radiotherapy or chemotherapy for improved efficacy. In phase I and II studies, Secord et al. [6] conducted studies combining Doxil®, PEG-coated nonthermosensitive liposomal doxorubicin, with whole abdomen hyperthermia on patients with refractory ovarian cancer. Liposomal doxorubicin combined with hyperthermia has been shown to increase both liposomal delivery and drug extravasation into tumor xenografts resulting in enhanced cytotoxic effects. Xia et al. [208] investigated the feasibility of hyperthermia combined with weekly chemoradiotherapy for patients with malignant pleural mesothelioma (MPM), a disease that affects the lining of the lungs, and estimated the efficacy of this regimen. Although complete response was not achieved in any of the 11 patients, partial response was achieved in 3 patients and the disease did not worsen in 6 patients. Prognosis for patients with MPM remains poor and, as such, patients require intensive treatment. Finally, Albregts et al. [2] have investigated the feasibility and toxicology of external deep locoregional hyperthermia combined with concurrent chemotherapy in localized primarily operable carcinoma of the thoracic oesophagus and gastro-oesophageal junction. The thermal data indicated that it was technically feasible to heat the oesophagus to a median temperature of 40.0°C with maximum

tumor temperatures considered adequate but suboptimal. One tried to evaluate tumor responses and found a complete remission rate of 9%, however, partial remission and progression are difficult to assess. In many such cases, the use of hyperthermia either alone or in conjunction with other modalities has significantly improved patient's quality of life.

20.6.2.2 Drug Delivery via Magnetic Targeting

Another possible and promising therapeutic application of SPIO nanoparticles is the site-specific delivery of drugs via a magnetic field (magnetic drug targeting, MDT) [55, 67, 183]. Because of the nonspecificity of chemotherapy and radiotherapy, there is considerable toxicity to normal tissue even under optimized conditions. MDT enjoys some advantages in that the drug-loaded SPIO can be guided to the target area through external magnetic fields to the desired site. The ability to deliver high effective dosages to specific sites in the human body is the ultimate goal of drug delivery research.

For drug delivery applications, these magnetic nanocarriers need to be water soluble, biocompatible, and nontoxic. Diameter, which affects the magnetic properties, charge, and surface chemistry, are very important and strongly affect both the blood circulation time and the bioavailability of the particles within the body. If one recalls, larger particles with a diameter greater than 200 nm are sequestered by the liver and spleen. Below 10 nm, USPIO will be quickly removed through extravasation and renal clearance. More over, particles over 5 μm will induce capillary blockade. Particles need be of optimal size ($\sim$10–100 nm) to prolong blood circulation times to enhance their magnetic targeting efficiency.

Magnetic fields are well suited for such biological applications as they do not interfere with most biological processes. However, there are still several problems associated with MDT in humans [153]. One such limitation is the influence of blood flow at the target site of SPIO accumulation. Stronger magnetic fields would be required to retain magnetic particles in large arteries. The linear velocity of blood in large arteries is 50–100 times faster than blood flow in capillaries ($\sim$0.5 cm/s). Yet another problem associated with MDT in humans is the depth of penetration by the magnetic field at the target site. Sites that are more than 2 cm deep in the body are difficult to target because the magnetic field strength decreases with distance [157]. In fact, through mathematical modeling, Grief and Richardson claim that it is impossible to specifically target internal organs using an externally applied field [62]. However, recent work by Takeda et al. [133, 176] describes the development of a novel drug delivery system using externally applied magnetic fields (using superconducting magnets) for targeting magnetic particles in blood vessels located deep inside the body.

Despite the challenges, progress has translated into clinical trials from in vitro [5, 47, 65, 109, 186] and in vivo [3, 4, 57, 93, 130] studies. The first clinical evaluations in human patients with MDT worldwide were reported by Lübbe et al. [123]. Following successful tolerance and efficacy results in animal experiments, studies were performed on 14 patients with advanced solid tumors (adenocarcinoma of the colon

or hypernephroma). Intravenous injection of epirubicine-loaded ferrofluids (particle size of 100 nm) were administered with bedside magnetic fields of approximately 0.8 T. The distance between the tumor surface and the magnets were also assured to be less than 0.5 cm. As a result, the magnetic particles were successfully directed into half of the patients after a 60–120 min application period confirmed by MRI, and histology. In a different clinical study [118], 11 patients with unsuccessful conventionally treated malignant tumors were treated by MDT and examined by MRI. The tumors of all 11 patients varied in location but were intentionally chosen for their superficial site. Diseases in these patients varied from thoracic wall carcinomata, metastasis of breast carcinomata, metastatic chondrosarcomata, histiocytoma, sarcoma, etc. Once again, Farmorubicin (epirubicine-loaded ferrofluid) was administered at field strength of ∼0.8 T. Overall, the tolerance of the magnetic drug targeting was very good. Within the surveillance period, three patients showed partial tumor response, five patients showed stable disease, and three patients showed progressive disease. It is evident that MDT does have great potential therapeutic benefit despite several limitations.

20.7 Conclusion

Magnetic nanoparticles have become an increasingly important tool in disease diagnosis and therapy. To date, most of the clinical use of magnetic nanoparticles has focused on SPIO due to their chemical stability, biocompatibility, and relative ease of production. However, the search for more efficient contrast agents with increased sensitivity has led to the development of novel SPIO and other magnetic nanoparticles with improved magnetic properties. These nanoparticles can now be extended to study biology at the cellular and even the molecular level in different endeavors including cell tracking, gene expression, and biomolecular recognition. In the case of MRI, many challenges still remain in pursuit of the ideal MR imaging probe with imaging ultrasensitivity and disease specificity. A major limitation is the loss of signal that occurs using SPIOs, creating 'black holes' that prevent direct anatomical MR evaluation of the tissue in question and make it difficult to discriminate between targeted molecules and cells and image artifacts. Development of novel imaging methods (e.g. SWIFT imaging, white marker method) can overcome these limitations by turning the SPIO probes to positive contrast agents. Although current clinically used contrast agents do not have active targeting characteristics, a lot of work is in progress on the functionalization of these particles in order to widen their diagnostic ability. Magnetic nanoparticle-aided drug delivery is still very much in its infancy. However, with continuing advancement in the field, nanomagnetism will continue to play a significant role in biomedical research and nanomedicine.

Abbreviations

Ab	antibody
AG	arabinogalactan

AOT	dioctyl sulfosuccinate sodium salt
CCK	cholecystokinin
α-CD	α-cyclodextrin
CEA	carcinoembryonic antigen
CLIO	cross-linked iron oxide
CNS	central nervous system
CT	computed tomography
DMAP	4-(dimethyl-amino) pyridine
DMSA	*meso*-2,3-dimercaptosuccinic acid
DSPE-PEG	1,2-distearoyl-*sn*-glycero-3-phosphoethanolamine-*N*-[methoxy(polyethylene glycol)]
EAE	experimental autoimmune encephalomyelitis
Gd-BOPTA	gadobenate dimeglumine
GI	gastrointestinal tract
GSH	glutathione
hCG	human chorionic gonadotropin
HSA	human serum albumin
IgG	Immunoglobulin G
mAb	monoclonal antibody
MDT	magnetic drug targeting
MRI	magnetic resonance imaging
MION	monocrystalline iron oxide nanoparticles
MEIO	magnetism-engineered iron oxide
MI	myocardial infarction
M_s	saturation magnetization
MSC	mesenchymal stem cells
MPM	malignant pleural mesothelioma
MPS	mononuclear phagocytic system
MPM	malignant pleural mesothelioma
OMP	oral magnetic particles
PCL-b-PEG	poly(ε-caprolactone)-b-poly(ethylene glycol)
PEG	polyethylene glycols
PEO	poly(ethylene oxide)
PLL	poly(L-lysine)
PPO	poly(propylene oxide)
PSA	polysialic acids
RES	reticuloendothelial system
RGD	arginine–glycine–aspartic acid containing synthetic peptide
SC	stem cells
SPIO	superparamagnetic iron oxide
SSPIO	standard superparamagnetic iron oxide
TAT	transactivator of transcription peptide
TCL-SPION	thermal cross-linked superparamagnetic iron oxide
USPIO	ultra-small superparamagnetic iron oxide
VCAM-1	vascular cell adhesion molecule-1

References

1. Ai, H., et al.: Magnetite-loaded polymeric micelles as ultrasensitive magnetic-resonance probes. Adv. Mater. **17**, 1949–1952 (2005)
2. Albregts, M., et al.: A feasibility study in oesophageal carcinoma using deep loco-regional hyperthermia combined with concurrent chemotherapy followed by surgery. Int. J. Hyperthermia **20**, 647–659 (2004)
3. Alexiou, C., et al.: Locoregional cancer treatment with magnetic drug targeting. Cancer Res. **60**, 6641–6648 (2000)
4. Alexiou, C., et al.: Magnetic drug targeting: biodistribution and dependency on magnetic field strength. J. Magn. Magn. Mater. **252**, 363–366 (2002)
5. Alexiou, C., et al.: In vitro and in vivo investigations of targeted chemotherapy with magnetic nanoparticles. J. Magn. Magn. Mater. **293**, 389–393 (2005)
6. Alvarez Secord, A., et al.: Phase I/II trial of intravenous Doxil® and whole abdomen hyperthermia in patients with refractory ovarian cancer. Int. J. Hyperthermia **21**, 333–347 (2005)
7. Amsalem, Y., et al.: Iron-oxide labeling and outcome of transplanted mesenchymal stem cells in the infarcted myocardium. Circulation **116(suppl. I)**, I-38–I-45 (2007)
8. Anastase, S., et al.: Affinity chromatography of human anti-dextran antibodies: isolation of two distinct populations. J. Chromatogr. B, Biomed. Sci. Appl. **686**, 141–150 (1996)
9. Anderson, S.A., et al.: Noninvasive MR imaging of magnetically labeled stem cells to directly identify neovasculature in a glioma model. Blood **105**, 420–425 (2005)
10. Anzai, Y., et al.: Initial clinical experience with dextran-coated superparamagnetic iron oxide for detection of lymph node metastases in patients with head and neck cancer. Radiology **192**, 709–715 (1994)
11. Anzai, Y., et al.: Initial clinical experience with dextran-coated superparamagnetic iron oxide for detection of lymph node metastases in patients with head and neck cancer. J. Magn. Reson. Imaging **7**, 75–81 (1997)
12. Anzai, Y., et al.: Evaluation of neck and body metastases to nodes with ferumoxtran 10-enhanced MR imaging: phase III safety and fficacy study. Radiology **228**, 777–788 (2003)
13. Arbab, A.S., et al.: Ferumoxides-enhanced double-echo T2-weighted MR imaging in differentiating metastases from nonsolid benign lesions of the liver. Radiology **225**, 151–158 (2002)
14. Arbab, A.S., et al.: Characterization of biophysical and metabolic properties of cells labeled with superparamagnetic iron oxide nanoparticles and transfection agent for cellular MR imaging. Radiology **229**, 838–846 (2003)
15. Arbab, A.S., et al.: In vivo trafficking and targeted delivery of magnetically labelled stem cells. Hum. Gene Ther. **15**, 351–360 (2004)
16. Arbab, A.S., et al.: Comparison of transfection agents in forming complexes with ferumoxides, cell labeling efficiency, and cellular viability. Mol. Imag. **3**, 24–32 (2004)
17. Arbab, A.S., et al.: Labeling of cells with ferumoxides-protamine sulfate complexes does not inhibit function or differentiation capacity of hematopoietic or mesenchymal stem cells. NMR Biomed. **18**, 553–559 (2005)
18. Arbab, A.S., et al.: Labeled endothelial progenitor cells trafficking to sites of tumor angiogenesis magnetic resonance imaging and confocal microscopy studies of magnetically. Stem Cells **24**, 671–678 (2006)
19. Arruebo, M., et al.: Antibody-functionalized hybrid superparamagnetic nanoparticles. Adv. Funct. Mater. **17**, 1473–1479 (2007)
20. Artemov, D., et al.: MR molecular imaging of the Her-2/neu receptor in breast cancer cells using targeted iron oxide nanoparticles. Magn. Reson. Med. **49**, 403–408 (2003)
21. Artemov, D., et al.: Magnetic resonance molecular imaging of the HER-2/neu receptor. Cancer Res. **63**, 2723–2727 (2003)
22. Babes, L., et al.: Synthesis of iron oxide nanoparticles used as MRI contrast agents: a parametric study. J. Colloid Interface Sci. **212**, 474–482 (1999)

23. Bach-Gansmo, T.: Ferrimagnetic susceptibility contrast agents. Acta Radiol. Suppl. **387**, 1–30 (1993)
24. Bach-Gansmo, T., et al.: Abdominal MRI using a negative contrast agent. Br. J. Radiol. **66**, 420–425 (1993)
25. Bayer HealthCare Pharmaceuticals: Feridex®. http://imaging.bayerhealthcare.com/html/feridex/index.html (2007). Accessed 5 November 2007
26. Bee, A., et al.: Synthesis of very fine maghemite particles. J. Magn. Magn. Mater. **149**, 6–9 (1995)
27. Belin, T., et al.: Influence of grain size, oxygen stoichiometry, and synthesis conditions on the γ-Fe_2O_3 vacancies ordering and lattice parameters. J. Solid State Chem. **163**, 459–465 (2002)
28. Ben-Hur, T., et al.: Serial in vivo MR tracking of magnetically labeled neural spheres transplanted in chronic EAE mice. Magn. Reson. Med. **57**, 164–171 (2007)
29. Bjørnerud, A., et al.: Assessment of T_1 and T_2^* effects in vivo and ex vivo using iron oxide nanoparticles in steady state—dependence on blood volume and water exchange. Magn. Reson. Med. **47**, 461–471 (2002)
30. Bonnemain, B.: Superparamagnetic agents in magnetic resonance imaging. Physicochemical characteristics and clinical application. A review. J. Drug Target. **6**, 167–174 (1998)
31. Bos, C., et al.: In vivo MR imaging of intravascularly injected magnetically labeled stem cells in rat kidney and liver. Radiology **233**, 781–789 (2004)
32. Boudghëne, F.P., et al.: Contribution of oral magnetic particles in MR imaging of the abdomen with spin-echo and gradient-echo sequences. J. Magn. Reson. Imaging **3**, 107–112 (1993)
33. Brusentsov, N.A., et al.: Evaluation of ferromagnetic fluids and suspensions for the site-specific radiofrequency-induced hyperthermia of MX11 sarcoma cells in vitro. J. Magn. Magn. Mater. **225**, 113–117 (2001)
34. Bulte, J.W.M., et al.: Neurotransplantation of magnetically labeled oligodendrocytes progenitors: magnetic resonance tracking of cell migration and myelination. Proc. Natl. Acad. Sci. **96**, 15256–15261 (1999)
35. Bulte, J.W.M. and Kraitchman, D.L.: Iron oxide MR contrast agents for molecular and cellular imaging. NMR Biomed. **17**, 484–499 (2004)
36. Butle, J.W., et al.: Specific MR imaging of human lymphocytes by monoclonal antibody-guided dextran-magnetite particles. Magn. Reson. Med. **25**, 148–157 (1992)
37. Cahill, K.S., et al.: Noninvasive monitoring and tracking of muscle stem cell transplant. Transplantation **78**, 1626–1633 (2004)
38. Carreño, T.G., et al.: Preparation of homogeneous Zn/Co mixed oxides by spray pyrolysis. Mater. Chem. Phys. **27**, 287–296 (1991)
39. Cerdan, S., et al.: Monoclonal antibody-coated magnetite particles as contrast agents in magnetic resonance imaging of tumors. Magn. Reson. Med. **12**, 151–163 (1989)
40. Cheng, F.-Y., et al.: Characterization of aqueous dispersions of Fe_3O_4 nanoparticles and their biomedical applications. Biomaterials **26**, 729–738 (2005)
41. Choi, H.S., et al.: Renal clearance of quantum dots. Nat. Biotechnol. **25**, 1165–1170 (2007)
42. Choi, J.-S., et al.: Biocompatible heterostructured nanoparticles for multimodal biological detection. J. Am. Chem. Soc. **128**, 15982–15983 (2006)
43. Corot, C., et al.: Recent advances in iron oxide nanocrystal technology for medical imaging. Adv. Drug Del. Rev. **58**, 1471–1504 (2006)
44. Daldrup-Link, H.E., et al.: Macromolecular contrast medium (Feruglose) versus small molecular contrast medium (Gadopentetate) enhanced magnetic resonance imaging: differentiation of benign and malignant breast lesions. Acad. Radiol. **10**, 1237–1246 (2003)
45. Damadian, R.: Tumor detection by nuclear magnetic resonance. Science **171**, 1151–1153 (1971)
46. Damadian, R.: Apparatus and method for detecting cancer in tissue. US Patent 3,789,832: February 5, 1974

47. Dandamudi, S. and Campbell, R.B.: The drug loading, cytotoxicty and tumor vascular targeting characteristics of magnetite in magnetic drug targeting. Biomaterials **28**, 4673–4683 (2007)
48. Decher, G.: Fuzzy nanoassemblies: toward layered polymeric multicomposites. Science **277**, 1232–1237 (1997)
49. Deng, Y., et al.: Preparation of magnetic polymeric particles via inverse microemulsion polymerization process. J. Magn. Magn. Mater. **257**, 69–78 (2003)
50. Duterloo, H.S.: Historic publication on the first use of magnets in orthodontics. Am. J. Orthod. Dentofacial Orthop. **108**, 15A–16A (1995)
51. Dutton, A.H., et al.: Iron-dextran antibody conjugates: general method for simultaneous staining of two components in high-resolution immunoelectron microscopy. Proc. Natl. Acad. Sci. **76**, 3392–3396 (1979)
52. Fajardo, L.F.: Pathological effects of hyperthermia in normal tissues. Cancer Res. **44(suppl.)**, 4826s–4835s (1984)
53. Fauconnier, N., et al.: Thiolation of maghemite nanoparticles by dimercaptosuccinic acid. J. Colloid Interface Sci. **194**, 427–433 (1997)
54. Fishbane, S., et al.: The safety of intravenous iron dextran in hemodialysis patients. Am. J. Kidney Dis. **28**, 529–534 (1996)
55. Forbes, Z.G., et al.: An approach to targeted drug delivery based on uniform magnetic fields. IEEE Trans. Magn. **39**, 3372–3377 (2003)
56. Funovics, M.A., et al.: MR imaging of the her2/neu and 9.2.27 tumor antigens using immunospecific contrast agents. Magn. Reson. Imaging **22**, 843–850 (2004)
57. Gallo, J.M., et al.: Targeting anticancer drugs to the brain: II. Physiological pharmacokinetic model of oxantrazole following intraarterial administration to rat glioma-2 (RG-2) bearing rats. J. Pharmacokin. Biopharm. **21**, 575–592 (1993)
58. Gittins, D.I. and Caruso, F.: Spontaneous phase transfer of nanoparticulate metals from organic to aqueous media. Angew. Chem. Int. Ed. **40**, 3001–3004 (2001)
59. Glöckl, G., et al.: The effect of field parameters, nanoparticle properties and immobilization on the specific heating power in magnetic particle hyperthermia. J. Phys.: Condens. Matter **18**, S2935–S2949 (2006)
60. Gomi, T., et al.: Evaluation of the changes in signals from the spleen using ferucarbotran. Radiat. Med. **25**, 135–138 (2007)
61. Goya, F.G., et al.: Static and dymanic magnetic properties of spherical magnetite nanoparticles. J. Appl. Phys. **94**, 3520–3528 (2003)
62. Grief, A.D. and Richardson, G.: Mathematical modelling of magnetically targeted drug delivery. J. Magn. Magn. Mater. **293**, 455–463 (2005)
63. Groman, E.V.: Biologically degradable superparamagnetic materials for use in clinical applications. US Patent 4,827,945: May 9, 1989
64. Gupta, A.K. and Wells, S.: Surface-modified superparamagnetic nanoparticles for drug delivery: preparation, characterization, and cytotoxicity. IEEE Trans. Nanobiosci. **3**, 66–73 (2004)
65. Gupta, A.K. and Curtis, A.S.G.: Surface modified superparamagnetic nanoparticles for drug delivery: interaction studies with human fibroblasts in culture. J. Mater. Sci.: Mater. Med. **15**, 493–496 (2004)
66. Gupta, A.K. and Gupta, M.: Cytotoxicity suppression and cellular uptake enhancement of surface modified magnetic nanoparticles. Biomaterials **26**, 1565–1573 (2005)
67. Gupta, A.K. and Gupta, M.: Synthesis and surface engineering of iron oxide nanoparticles for biomedical applications. Biomaterials **26**, 3995–4021 (2005)
68. Guzman, R., et al.: Long-term monitoring of transplanted human neural stem cells in developmental and pathological contexts with MRI. Proc. Natl. Acad. Sci. **104**, 10211–10216 (2007)
69. Häfeli, U.: The History of Magnetism in Medicine. In: Andrä, W. and Nowak, H. (eds.) Magnetism in Medicine: A Handbook, Second Edition, pp. 1–25. Wiley-VCH Verlag GmbH & Co. KGaA, Weinheim (2007)

70. Hahn, P.F., et al.: First clinical trials of a new superparamagnetic iron oxide for the use as an oral gastrointestinal contrast agent in MR imaging. Radiology **175**, 695–700 (1990)
71. Harisinghani, M.G., et al.: Splenic imaging with ultrasmall superparamagnetic iron oxide ferumoxtran-10 (AMI-7227): preliminary observations. J. Comput. Assist. Tomogr. **25**, 770–776 (2001)
72. Harisinghani, M.G., et al.: Noninvasive detection of clinically occult lymph-node metastases in prostate cancer. N. Engl. J. Med. **348**, 2491–2499 (2003)
73. Hasegawa, M. and Hokkoku, S.: Magnetic iron oxide-dextran complex and process for its production. US Patent 4,101,435: July 18, 1978
74. Hergt, R., et al.: Magnetic particle hyperthermia: nanoparticle magnetism and materials development for cancer therapy. J. Phys.: Condens. Matter **18**, S2919–S2934 (2006)
75. Hill, J.M., et al.: Serial cardiac magnetic resonance imaging of injected mesenchymal stem cells. Circulation **108**, 1009–1014 (2003)
76. Himes, N., et al.: In vivo MRI of embryonic stem cells in a mouse model of myocardial infarction. Magn. Reson. Med. **52**, 1214–1219 (2004)
77. Hogemann, D., et al.: High throughput magnetic resonance imaging for evaluating targeted nanoparticle probes. Bioconjug. Chem. **13**, 116–121 (2002)
78. Hong, R., et al.: Comparison of schemes for preparing magnetic Fe_3O_4 nanoparticles. China Particuology **5**, 186–191 (2007)
79. Hu, D.E., et al.: Monitoring T-lymphocyte trafficking in tumors undergoing immune rejection. Magn. Reson. Med. **54**, 1473–1479 (2005)
80. Hyeon, T., et al.: Synthesis of highly crystalline and monodisperse maghemite nanocrystallites without a size-selection process. J. Am. Chem. Soc. **123**, 12798–12801 (2001)
81. Hyeon, T., et al.: Synthesis of highly crystalline and monodisperse cobalt ferrite nanocrystals J. Phys. Chem. B **106**, 6831–6833 (2002)
82. Ichikawa, T., et al.: MRI of transgene expression: correlation to therapeutic gene expression. Neoplasia **4**, 523–530 (2002)
83. Igartua, M., et al.: Development and characterization of solid lipid nanoparticles loaded with magnetite. Int. J. Pharm. **233**, 149–157 (2002)
84. Ittrich, H., et al.: In vivo magnetic resonance imaging of iron oxide-labeled, arterially-injected mesenchymal stem cells in kidneys of rats with acute ischemic kidney injury: detection and monitoring at 3T. J. Magn. Reson. Imag. **25**, 1179–1191 (2007)
85. Jacobsen, T.F., et al.: Oral magnetic particles (ferristene) as a contrast medium in abdominal magnetic resonance imaging. Acad. Radiol. **3**, 571–580 (1996)
86. Jendelova, P., et al.: Magnetic resonance tracking of transplanted bone marrow and embryonic stem cells labeled by iron oxide nanoparticles in rat brain and spinal cord. J. Neurosci. Res. **76**, 232–243 (2004)
87. Johannsen, M., et al.: Clinical hyperthermia of prostate cancer using magnetic nanoparticles: presentation of a new interstitial technique. Int. J. Hyperthermia **21**, 637–647 (2005)
88. Johansson, L.O., et al.: A targeted contrast agent for magnetic resonance imaging of thrombus: implications of spatial resolution. J. Magn. Reson. Imaging **13**, 615–618 (2001)
89. Josephson, L., et al.: High-efficiency intracellular magnetic labeling with novel superparamagnetic-tat peptide conjugates. Bioconjug. Chem. **10**, 186–191 (1999)
90. Ju, S., et al.: In Vivo MR tracking of mesenchymal stem cells in rat liver after intrasplenic transplantation. Radiology **245**, 206–215 (2007)
91. Jun, Y.-W., et al.: Nanoscale size effect of magnetic nanocrystals and their utilization for cancer diagnosis via magnetic resonance imaging. J. Am. Chem. Soc. **127**, 5732–5733 (2005)
92. Jung, C.W. and Jacobs, P.: Physical and chemical properties of superparamagnetic iron oxide MR contrast agents: ferumoxides, ferumoxtran, ferumoxsil. Magn. Reson. Imaging **13**, 661–674 (1995)
93. Jurgons, R., et al.: Drug loaded magnetic nanoparticles for cancer therapy. J. Phys.: Condens. Matter **18**, S2893–S2902 (2006)
94. Kanematsu, M., et al.: Imaging liver metastases: review and update. Eur. J. Radiol. **58**, 217–228 (2006)

95. Kang, E., et al.: Direct synthesis of highly crystalline and monodisperse manganese ferrite nanocrystals. J. Phys. Chem. B **108**, 13932–13935 (2004)
96. Kang, H.W., et al.: Magnetic resonance imaging of inducible E-selectin expression in human endothelial cell culture. Bioconjug. Chem. **13**, 122–127 (2002)
97. Kang, Y.S., et al.: Synthesis and characterization of nanometer-size Fe_3O_4 and γ-Fe_2O_3 particles. Chem. Mater. **8**, 2209–2211 (1996)
98. Kato, H., et al.: Ferumoxide-enhanced MR imaging of hepatocellular carcinoma: correlation with histologic tumor grade and tumor vascularity. J. Magn. Reson. Imaging **19**, 76–81 (2004)
99. Kehagias, D.T., et al.: Diagnostic efficacy and safety of MRI of the liver with superparamagnetic iron oxide particles (SH U 555 A). J. Magn. Reson. Imaging **14**, 595–601 (2001)
100. Kelly, K.A., et al.: Detection of vascular adhesion molecule-1 expression using a novel multimodal nanoparticle. Circ. Res. **96**, 327–336 (2005)
101. Kim, D.K., et al.: Synthesis and characterization of surfactant-coated superparamagnetic monodispersed iron oxide nanoparticles. J. Magn. Magn. Mater. **225**, 30–36 (2001)
102. Kim, S.-H., et al.: Fabrication and estimation of Au-coated Fe_3O_4 nanocomposite powders for the separation and purification of biomolecules. Mater. Sci. Eng. A **449–451**, 386–388 (2007)
103. Kim, Y.K., et al.: Detection of liver metastases: gadobenate dimeglumine-enhanced three-dimensional dynamic phases and one-hour delayed phase MR imaging versus superparamagnetic iron oxide-enhanced MR imaging. Eur. Radiol. **15**, 220–228 (2005)
104. Kircher, M.F., et al.: In vivo high resolution three-dimensional imaging of antigen-specific cytotoxic T-lymphocyte trafficking to tumors. Cancer Res. **63**, 6838–6846 (2003)
105. Koh, D.-M., et al.: New horizons in oncologic imaging. N. Engl. J. Med. **348**, 2487–2488 (2003)
106. Kopp, A., et al.: MR imaging of the liver with resovist: safety,efficacy, and pharmacodynamic properties. Radiology **204**, 749–756 (1997)
107. Kraitchman, D.L., et al.: In vivo magnetic resonance imaging of mesenchymal stem cells in myocardial infarction. Circulation **107**, 2290–2293 (2003)
108. Kresse, M., et al.: Targeting of ultrasmall superparamagnetic iron oxide (USPIO) particles to tumor cells in vivo by using transferrin receptor pathways. Magn. Reson. Med. **40**, 236–242 (1998)
109. Kullberg, M., et al.: Improved drug delivery to cancer cells: a method using magnetoliposomes that target epidermal growth factor receptors. Med. Hypoth. **64**, 468–470 (2005)
110. Laghi, A., et al.: Oral contrast agents for magnetic resonance imaging of the bowel. Top. Magn. Reson. Imaging **13**, 389–396 (2002)
111. Lawaczeck, R., et al.: Superparamagnetic iron oxide particles: contrast media for magnetic resonance imaging. Appl. Organometal. Chem. **18**, 506–513 (2004)
112. Lee, H., et al.: Thermally cross-linked superparamagnetic iron oxide nanoparticles: synthesis and application as a dual imaging probe for cancer in vivo. J. Am. Chem. Soc. **129**, 12739–12745 (2007)
113. Lee, J.-H., et al.: Dual-mode nanoparticle probes for high-performance magnetic resonance and fluorescence imaging of neuroblastoma. Angew. Chem. Int. Ed. **45**, 8160–8162 (2006)
114. Lee, J.-H., et al.: Artificially engineered magnetic nanoparticles for ultra-sensitive molecular imaging. Nat. Med. **13**, 95–99 (2007)
115. Lee, S.-J., et al.: Synthesis and characterization of superparamagnetic maghemite nanoparticles prepared by coprecipitation technique. J. Magn. Magn. Mater. **282**, 147–150 (2004)
116. Lee, Y., et al.: Large-scale synthesis of uniform and crystalline magnetite nanoparticles using reverse micelles as nanoreactors under reflux conditions. Adv. Funct. Mater. **15**, 503–509 (2005)
117. Lefebure, S., et al.: Monodisperse magnetic nanoparticles: preparation and dispersion in water and oils. J. Mater. Res. **13**, 2975–2981 (1998)

118. Lemke, A.-J., et al.: MRI after magnetic drug targeting in patients with advanced solid malignant tumors. Eur. Radiol. **14**, 1949–1955 (2004)
119. Lewin, M., et al.: Tat peptide-derivatized magnetic nanoparticles allow in vivo tracking and recovery of progenitor cells. Nat. Biotechnol. **18**, 410–414 (2000)
120. Li, S., et al.: Structured materials syntheses in a self-assembled surfactant mesophase. Colloids Surf. A **174**, 275–281 (2000)
121. Livesay, B.R.: 9th International Conference on rare earth magnets and their applications. (1987)
122. López, A., et al.: Magnetic properties of γ-Fe_2O_3 small particles prepared by spray pyrolysis. J. Magn. Magn. Mater. **140–144**, 383–384 (1995)
123. Lübbe, A.S., et al.: Clinical applications of magnetic drug targeting. J. Surg. Res. **95**, 200–206 (2001)
124. MacVicar, D., et al.: Phase III trial of oral magnetic particles in MRI of abdomen and pelvis. Clin. Radiol. **47**, 183–188 (1993)
125. Matuszewski, L., et al.: Cell tagging with clinically approved iron oxides: feasibility and effect of lipofection, particle size, and surface coating on labeling efficiency. Radiology **235**, 155–161 (2005)
126. McLachlan, S.J., et al.: Phase I clinical evaluation of a new iron oxide MR contrast agent. J. Magn. Reson. Imaging **43**, 301–307 (1994)
127. Metz, S., et al.: Capacity of human monocytes to phagocytose approved iron oxide MR contrast agents in vitro. Eur. Radiol. **14**, 1851–1858 (2004)
128. Moore, A., et al.: Measuring transferrin receptor gene expression by NMR imaging. Biochim. Biophys. Acta **1402**, 239–249 (1998)
129. Moore, A., et al.: In vivo targeting of underglycosylated MUC-1 tumor antigen using a multimodal imaging probe. Cancer Res. **64**, 1821–1827 (2004)
130. Mykhaylyk, O., et al.: Doxorubicin magnetic conjugate targeting upon intravenous injection into mice: high gradient magnetic field inhibits the clearance of nanoparticles from the blood. J. Magn. Magn. Mater. **293**, 473–482 (2005)
131. Namkung, S., et al.: Superparamagnetic iron oxide (SPIO)-enhanced liver MRI with ferucarbotran: efficacy for characterization of focal liver lesions. J. Magn. Reson. Imaging **25**, 755–765 (2007)
132. Nedkov, I., et al.: Surface oxidation, size and shape of nano-sized magnetite obtained by co-precipitation. J. Magn. Magn. Mater. **300**, 358–367 (2006)
133. Nishijima, S., et al.: A study on magnetically targeted drug delivery system using superconducting magnet. Physica C **463–465**, 1311–1314 (2007)
134. Nishimura, H., et al.: Preoperative esophageal cancer staging: magnetic resonance imaging of lymph node with ferumoxtran-10, an ultrasmall superparamagnetic iron oxide. J. Am. Coll. Surg. **202**, 604–611 (2006)
135. Oude Engberink, R.D., et al.: Comparison of SPIO and USPIO for in vitro labeling of human monocytes: MR detection and cell function. Radiology **243**, 467–474 (2007)
136. Papell, S.S.: Low viscosity magnetic fluid obtained by the colloidal suspension of magnetic particles. US Patent 3,215,572: November 2, 1965
137. Park, H.-Y., et al.: Fabrication of magnetic core@shell Fe oxide@Au nanoparticles for interfacial bioactivity and bio-separation. Langmuir **23**, 9050–9056 (2007)
138. Park, J., et al.: Ultra-large-scale syntheses of monodisperse nanocrystals. Nat. Mater. **3**, 891–895 (2004)
139. Park, J., et al.: One-nanometer-scale size-controlled synthesis of monodisperse magnetic iron oxide nanoparticles. Angew. Chem. Int. Ed. **44**, 2872–2877 (2005)
140. Pellegrino, T., et al.: Hydrophobic nanocrystals coated with an amphiphilic polymer shell: a general route to water soluble nanocrystals. Nano Lett. **4**, 703–707 (2004)
141. Pillai, V., et al.: Preparation of nanoparticles of silver halides, superconductors and magnetic materials using water-in-oil microemulsions as nano-reactors. Adv. Colloid Interface Sci. **55**, 241–269 (1995)

142. Pirko, I., et al.: In vivo magnetic resonance imaging of immune cells in the central nervous system with superparamagnetic antibodies. FASEB **18**, 179–181 (2004)
143. Qin, J., et al.: A high-performance magnetic resonance imaging T_2 contrast agent. Adv. Mater. **19**, 1874–1878 (2007)
144. Raaphorst, G.P.: Fundamental aspects of hyperthermic biology. In: Field, S.B. and Hand, J.W. (eds.) An Introduction to the Practical Aspects of Clinical Hyperthermia, pp. 10–54. Taylor and Francis, London (1990)
145. Rad, A.M., et al.: Quantification of superparamagnetic iron oxide (SPIO)-labeled cells using MRI. J. Magn. Reson. Imag. **26**, 366–374 (2007)
146. Reimer, P., et al.: Receptor imaging: application to MR imaging of liver cancer. Radiology **177**, 729–734 (1990)
147. Reimer, P., et al.: Receptor-directed contrast agents for MR imaging: preclinical evaluation with affinity assays. Radiology **182**, 565–569 (1992)
148. Reimer, P., et al.: Pancreatic receptors: initial feasibility studies with a targeted contrast agent for MR imaging. Radiology **193**, 527–531 (1994)
149. Reimer, P. and Tombach, B.: Hepatic MRI with SPIO: detection and characterization of focal liver lesions. Eur. Radiol. **8**, 1198–1204 (1998)
150. Reimer, P. and Balzer, T.: Ferucarbotran (Resovist): a new clinically approved RES-specific contrast agent for contrast-enhanced MRI of the liver: properties, clinical development, and applications. Eur. Radiol. **13**, 1266–1276 (2003)
151. Remsen, L.G., et al.: MR of carcinoma-specific monoclonal antibody conjugated to monocrystalline iron oxide nanoparticles: the potential for noninvasive diagnosis. Am. J. Neuroradiol. **17**, 411–418 (1996)
152. Renshaw, P.F., et al.: Immunospecific NMR contrast agents. Magn. Reson. Imaging **4**, 351–357 (1986)
153. Ritter, J.A., et al.: Application of high gradient magnetic separation principles to magnetic drug targeting. J. Magn. Magn. Mater. **280**, 184–201 (2004)
154. Rockenberger, J., et al.: A new nonhydrolytic single-precursor approach to surfactant-capped nanocrystals of transition metal oxides. J. Am. Chem. Soc. **121**, 11595–11596 (1999)
155. Roger, J., et al.: Behavior of aqueous ferrofluids in presence of amino acids. Eur. J. Solid State Inorg. Chem. **26**, 475–488 (1989)
156. Rohrer, M., et al.: Comparison of magnetic properties of MRI contrast media solutions at different magnetic field strengths. Invest. Radiol. **40**, 715–724 (2005)
157. Rudge, S.R., et al.: Preparation, characterization, and performance of magnetic iron-carbon composite microparticles for chemotherapy. Biomaterials **21**, 1411–1420 (2000)
158. Sanderson, C.J. and Wilson, D.V.: A simple method for coupling proteins to insoluble polysaccharides. Immunology **20**, 1061–1065 (1971)
159. Savellano, M.D. and Hasan, T.: Targeting cells that overexpress the epidermal growth factor receptor with polyethylene glycolated BPD verteporfin photosensitizer immunoconjugates. Photochem. Photobiol. **77**, 431–439 (2003)
160. Schellenberger, E.A., et al.: Surface-functionalized nanoparticle library yields probes for apoptotic cells. Chem. Bio. Chem. **5**, 275–279 (2004)
161. Schulze, E., et al.: Cellular uptake and trafficking of a prototypical magnetic iron oxide label in vitro. Invest. Radiol. **30**, 604–610 (1995)
162. Seip, C.T., et al.: Magnetic properties of a series of ferrite nanoparticles synthesized in reverse micelles. IEEE Trans. Magn. **34**, 1111–1113 (1998)
163. Semelka, R.C. and Helmberger, T.K.: Contrast agents for MR imaging of the liver. Radiology **218**, 27–38 (2001)
164. Seo, W.S., et al.: FeCo/graphitic-shell nanocrystals as advanced magnetic-resonance-imaging and near-infrared agents. Nat. Mater. **5**, 971–976 (2006)
165. Shen, T., et al.: Monocrystalline iron oxide nanocompounds (MION): physicochemical properties. MRM **29**, 599–604 (1993)
166. Shen, T.T., et al.: Magnetically labeled secretin retains receptor affinity to pancreas acinar cells. Bioconjug. Chem. **7**, 311–316 (1996)

167. Simon, G.H., et al.: Ultrasmall supraparamagnetic iron oxide-enhanced magnetic resonance imaging of antigen-induced arthritis. A comparative study between SHU 555 C, Ferumoxtran-10, and Ferumoxytol. Invest. Radiol. **41**, 45–51 (2006)
168. Sminia, P., et al.: Effect of hyperthermia on the central nervous system. Int. J. Hyperthermia **10**, 1–130 (1994)
169. Stark, D.D., et al.: Superparamagnetic iron oxide: clinical application as a contrast agent for MR imaging of the liver. Radiology **168**, 297–301 (1988)
170. Stolnik, S., et al.: Long circulating microparticulate drug carriers. Adv. Drug Del. Rev. **16**, 195–214 (1995)
171. Sun, R., et al.: Physical and biological characterization of superparamagnetic iron oxide- and ultrasmall superparamagnetic iron oxide-labeled cells. Invest. Radiol. **40**, 504–513 (2005)
172. Sun, S. and Zeng, H.: Size-controlled synthesis of magnetite nanoparticles. J. Am. Chem. Soc. **124**, 8204–8205 (2002)
173. Sun, S., et al.: Monodisperse MFe_2O_4 (M=Fe, Co, Mn) nanoparticles. J. Am. Chem. Soc. **126**, 273–279 (2004)
174. Suslick, K.S., et al.: Sonochemical synthesis of iron colloids. J. Am. Chem. Soc. **118**, 11960–11961 (1996)
175. Suwa, T., et al.: Magnetic Resonance imaging of esophageal squamous cell carcinoma using magnetite particles coated with anti-epidermal growth factor receptor antibody. Int. J. Cancer **75**, 626–634 (1998)
176. Takeda, S., et al.: Development of magnetically targeted drug delivery system using superconducting magnet. J. Magn. Magn. Mater. **311**, 367–371 (2007)
177. Tang, J., et al.: Magnetite Fe_3O_4 nanocrystals: spectroscopic observation of aqueous oxidation kinetics. J. Phys. Chem. B **107**, 7501–7506 (2003)
178. Taupitz, M., et al.: Phase I clinical evaluation of citrate-coated monocrystalline very small superparamagnetic iron oxide particles as a new contrast medium for magnetic resonance imaging. Invest. Radiol. **39**, 394–405 (2004)
179. Thorek, D.L.J., et al.: Superparamagnetic iron oxide nanoparticle probes for molecular imaging. Ann. Biomed. Eng. **34**, 23–38 (2006)
180. Tiefenauer, L.X., et al.: Antibody-magnetite nanoparticles: in vitro characterization of a potential tumor-specific contrast agent for magnetic resonance imaging. Bioconjug. Chem. **4**, 347–352 (1993)
181. Tiefenauer, L.X., et al.: In vivo evaluation of magnetite nanoparticles for use as a tumor contrast agent in MRI. Magn. Reson. Imaging **14**, 391–402 (1996)
182. Toma, A., et al.: Monoclonal antibody A7-superparamagnetic iron oxide as contrast agent of MR imaging of rectal carcinoma. Br. J. Cancer **93**, 131–136 (2005)
183. Torchilin, V.P.: Drug targeting. Eur. J. Pharm. Sci. **11(Suppl. 2)**, S81–S91 (2000)
184. Treleaven, J.G., et al.: Removal of neuroblastoma cells from bone marrow with monoclonal antibodies conjugated to magnetic microspheres. The Lancet **14**, 70–73 (1984)
185. Treleaven, J.G.: Bone marrow purging: an appraisal of immunological and non-immunological methods. Adv. Drug Del. Rev. **2/3**, 253–269 (1988)
186. Udrea, L.E., et al.: An in vitro study of magnetic particle targeting in small blood vessels. Phys. Med. Biol. **51**, 4869–4881 (2006)
187. van der Zee, J.: Heating the patient: a promising approach? Ann. Oncol. **13**, 1173–1184 (2002)
188. Veintemillas-Verdaguer, S., et al.: Effect of the oxidation conditions on the maghemites production by laser pyrolysis. J. Appl. Organometal. Chem. **15**, 365–372 (2001)
189. Vlahos, L., et al.: A comparative study between Gd-DTPA and oral magnetic particles (OMP) as gastrointestinal (GI) contrast agents for MRI of the abdomen. Magn. Reson. Imaging **12**, 719–726 (1994)
190. Wadghiri, Y.Z., et al.: Detection of alzheimer's amyloid in transgenic mice using magnetic resonance microimaging. Magn. Reson. Med. **50**, 293–302 (2003)
191. Walter, G.A., et al.: Noninvasive monitoring of stem cell transfer for muscle disorders. Magn. Reson. Med. **51**, 273–277 (2004)

192. Wang, F.H., et al.: Magnetic resonance tracking of nanoparticle labelled neural stem cells in a rat's spinal cord. Nanotechnol. **17**, 1911–1915 (2006)
193. Wang, J., et al.: Stepwise directing of nanocrystals to self-assemble at water/oil interfaces. Angew. Chem. Int. Ed. **45**, 7963–7966 (2006)
194. Wang, X., et al.: The heating effect of magnetic fluids in an alternating magnetic field. J. Magn. Magn. Mater. **293**, 334–340 (2005)
195. Wang, Y.-X.J., et al.: Superparamagnetic iron oxide contrast agents: physicochemical characteristics and applications in MR imaging. Eur. Radiol. **11**, 2319–2331 (2001)
196. Wang, Y., et al.: "Pulling" nanoparticles into water: phase transfer of oleic acid stabilized monodisperse nanoparticles into aqueous solutions of α-cyclodextrin. Nano Lett. **3**, 1555–1559 (2003)
197. Weissleder, R., et al.: Superparamagnetic iron oxide: pharmacokinetics and toxicity. AJR **152**, 167–173 (1989)
198. Weissleder, R., et al.: Ultrasmall superparamagnetic iron oxide: characterization of a new class of contrast agents for MR imaging. Radiology **175**, 489–493 (1990)
199. Weissleder, R., et al.: MR receptor imaging: ultrasmall iron oxide particles targeted to asialoglycoprotein receptors. AJR **155**, 1161–1167 (1990)
200. Weissleder, R., et al.: Polyclonal human immunoglobulin G labeled with polymeric iron oxide: antibody MR imaging. Radiology **181**, 245–249 (1991)
201. Weissleder, R., et al.: Antimyosin-labeled monocrystalline iron oxide allows detection of myocardial infarct: MR antibody imaging. Radiology **182**, 381–385 (1992)
202. Weissleder, R., et al.: Long-circulating iron oxides for MR imaging. Adv. Drug Del. Rev. **16**, 321–334 (1995)
203. Weissleder, R., et al.: In vivo magnetic resonance imaging of transgene expression. Nat. Med. **6**, 351–355 (2000)
204. Weissleder, R., et al.: Cell-specific targeting of nanoparticles by multivalent attachment of small molecules. Nat. Biotechnol. **23**, 1418–1423 (2005)
205. Whitehead, R.A.: Magnetic particles for use in separations. US Patent 4,554,088: November 19, 1985
206. Wondergem, J., et al.: Effects of local hyperthermia on the motor function of the rat sciatic nerve. Int. J. Radiat. Biol. **53**, 429–439 (1988)
207. Wunderbaldinger, P., et al.: Crosslinked iron oxides (CLIO): a new platform for the development of targeted MR contrast agents. Acad. Radiol. **9(suppl. 2)**, S304–S306 (2002)
208. Xia, H., et al.: Hyperthermia combined with intra-thoracic chemotherapy and radiotherapy for malignant pleural mesothelioma. Int. J. Hyperthermia **22**, 613–621 (2006)
209. Xu, Z., et al.: Magnetic core/shell Fe_3O_4/Au and Fe_3O_4/Au/Ag nanoparticles with tunable plasmonic properties. J. Am. Chem. Soc. **129**, 8698–8699 (2007)
210. Zeng, H., et al.: Shape-controlled synthesis and shape-induced texture of $MnFe_2O_4$ nanoparticles. J. Am. Chem. Soc. **126**, 11458–11459 (2004)
211. Zhang, C., et al.: Silica- and alkoxysilane-coated ultrasmall superparamagnetic iron oxide particles: a promising tool to label cells for magnetic resonance imaging. Langmuir **23**, 1427–1434 (2007)
212. Zhang, Y., et al.: Surface modification of superparamagnetic magnetite nanoparticles and their intracellular uptake. Biomaterials **23**, 1553–1561 (2002)
213. Zhang, Y. and Zhang, J.: Surface modification of monodisperse magnetite nanoparticles for improved intracellular uptake to breast cancer cells. J. Colloid Interface Sci. **283**, 352–357 (2005)
214. Zhao, M., et al.: Non-invasive detection of apoptosis using magnetic resonance imaging and a targeted contrast agent. Nat. Med. **7**, 1241–1244 (2001)
215. Zhao, M., et al.: Differential conjugation of tat peptide to superparamagnetic nanoparticles and Its effect on cellular uptake. Bioconjug. Chem. **13**, 840–844 (2002)
216. Zinderman, C.E., et al.: Anaphylactoid reactions to dextran 40 and 70: reports to the United States Food and Drug Administration, 1969 to 2004. J. Vasc. Surg. **43**, 1004–1009 (2006)